

*ARMY RESEARCH LABORATORY*



**Communication Channel Estimation and Waveform Design:  
Time Delay Estimation on Parallel, Flat Fading Channels**

**by Richard J. Kozick and Brian M. Sadler**

**ARL-TR-5046**

**February 2010**

## **NOTICES**

### **Disclaimers**

The findings in this report are not to be construed as an official Department of the Army position unless so designated by other authorized documents.

Citation of manufacturer's or trade names does not constitute an official endorsement or approval of the use thereof.

Destroy this report when it is no longer needed. Do not return it to the originator.

# **Army Research Laboratory**

Adelphi, MD 20783-1197

---

---

**ARL-TR-5046**

**February 2010**

---

## **Communication Channel Estimation and Waveform Design: Time Delay Estimation on Parallel, Flat Fading Channels**

**Richard J. Kozick and Brian M. Sadler**  
**Computational and Information Sciences Directorate, ARL**

# REPORT DOCUMENTATION PAGE

*Form Approved*  
OMB No. 0704-0188

Public reporting burden for this collection of information is estimated to average 1 hour per response, including the time for reviewing instructions, searching existing data sources, gathering and maintaining the data needed, and completing and reviewing the collection information. Send comments regarding this burden estimate or any other aspect of this collection of information, including suggestions for reducing the burden, to Department of Defense, Washington Headquarters Services, Directorate for Information Operations and Reports (0704-0188), 1215 Jefferson Davis Highway, Suite 1204, Arlington, VA 22202-4302. Respondents should be aware that notwithstanding any other provision of law, no person shall be subject to any penalty for failing to comply with a collection of information if it does not display a currently valid OMB control number.

**PLEASE DO NOT RETURN YOUR FORM TO THE ABOVE ADDRESS.**

<b>1. REPORT DATE (DD-MM-YYYY)</b> February 2010		<b>2. REPORT TYPE</b>		<b>3. DATES COVERED (From - To)</b> FY09	
<b>4. TITLE AND SUBTITLE</b> Communication Channel Estimation and Waveform Design: Time Delay Estimation on Parallel, Flat Fading Channels				<b>5a. CONTRACT NUMBER</b>	
				<b>5b. GRANT NUMBER</b>	
				<b>5c. PROGRAM ELEMENT NUMBER</b>	
<b>6. AUTHOR(S)</b> Richard J. Kozick and Brian M. Sadler				<b>5d. PROJECT NUMBER</b>	
				<b>5e. TASK NUMBER</b>	
				<b>5f. WORK UNIT NUMBER</b>	
<b>7. PERFORMING ORGANIZATION NAME(S) AND ADDRESS(ES)</b> U.S. Army Research Laboratory ATTN: RDRL-CIN-T 2800 Powder Mill Road Adelphi, MD 20783-1197				<b>8. PERFORMING ORGANIZATION REPORT NUMBER</b>  ARL-TR-5046	
<b>9. SPONSORING/MONITORING AGENCY NAME(S) AND ADDRESS(ES)</b>				<b>10. SPONSOR/MONITOR'S ACRONYM(S)</b>	
				<b>11. SPONSOR/MONITOR'S REPORT NUMBER(S)</b>	
<b>12. DISTRIBUTION/AVAILABILITY STATEMENT</b> Approved for public release; distribution unlimited.					
<b>13. SUPPLEMENTARY NOTES</b>					
<b>14. ABSTRACT</b> A review of performance bounds for time-delay estimation (TDE) is presented, including a discussion of current trends. Then the problem of waveform design for TDE using frequency-hopping (FH) waveforms is analyzed to study the effects of fading and diversity on TDE over parallel channels with flat, Rayleigh fading. We present the maximum likelihood estimator (MLE), the Cramér-Rao bound (CRB), and the Ziv-Zakai bound on TDE for several different approaches to modeling the fading channels. Computer simulations of the mean-squared error (MSE) of the MLEs indicate that the ZZB provides a significantly tighter bound than the CRB, and the ZZB exhibits a SNR-threshold region that agrees with the MLE performance.					
<b>15. SUBJECT TERMS</b> Wireless communications, time delay estimation					
<b>16. SECURITY CLASSIFICATION OF:</b>			<b>17. LIMITATION OF ABSTRACT</b>  UU	<b>18. NUMBER OF PAGES</b>  50	<b>19a. NAME OF RESPONSIBLE PERSON</b> Brian Sadler
<b>a. REPORT</b> Unclassified	<b>b. ABSTRACT</b> Unclassified	<b>c. THIS PAGE</b> Unclassified			<b>19b. TELEPHONE NUMBER (Include area code)</b> (301) 394-1239

# Contents

<b>1. Introduction</b>	<b>1</b>
<b>2. A Survey of Time Delay Estimation Performance Bounds</b>	<b>2</b>
2.1 Cramér-Rao Bound . . . . .	4
2.2 Ziv-Zakai and Weiss-Weinstein Bounds . . . . .	6
2.3 Impact of Coherence . . . . .	9
2.4 Sensor Networks and Geolocation . . . . .	13
<b>3. TDE on Parallel, Flat Fading Channels</b>	<b>13</b>
<b>4. Signal Model</b>	<b>14</b>
<b>5. TDE Estimators and Bounds</b>	<b>19</b>
5.1 Maximum Likelihood Estimators . . . . .	19
5.2 Cramér-Rao Bounds . . . . .	20
5.3 Ziv-Zakai Bounds . . . . .	23
<b>6. Examples and Simulation Results</b>	<b>28</b>
6.1 One Symbol Per Hop . . . . .	28
6.2 Multiple Symbols Per Hop . . . . .	31
<b>7. Concluding Remarks</b>	<b>34</b>
<b>8. References</b>	<b>35</b>
<b>List of Symbols, Abbreviations, and Acronyms</b>	<b>40</b>



---

## List of Figures

1	(a) Threshold coherence value from equation 32 versus time-bandwidth product TB for several values of fractional bandwidth $B/\omega_c$ with $S/N_o \rightarrow \infty$ . (b) Comparison of simulated RMS error for TDE with CRBs and threshold coherence value for signals with bandwidth $B/(2\pi) = 30$ Hz centered at $\omega_c/(2\pi) = 100$ Hz. . . . .	12
2	Comparison of CRB, ZZB, and MSE for case of $L = 1$ symbol per hop for $N = 1, 3$ , and 5 channels . . . . .	29
3	CRB and ZZB for case of $L = 1$ symbol per hop for $N = 1, 2, \dots, 8$ . (a) Known channel with fixed gain; (b) average of case (a) over Rayleigh channels, so the channel gain is known on each realization and used in a coherent matched filter; and (c) Rayleigh channels with noncoherent matched filters . . . . .	30
4	CRB and ZZB for fixed total number of symbols $Q = LN = 80$ , for $N = 1, 2, 4, 8$ so $L = 80, 40, 20, 10$ to show the tradeoff of shorter dwells per hop and more hops. (a) Known channel with fixed gain (channel model 1); (b) average of case (a) over Rayleigh channels, so the channel gain is known on each realization and used in a coherent matched filter (channel model 1A); and (c) Rayleigh channels with noncoherent matched filters (channel model 3) . . . . .	32
5	Comparison of CRB, ZZB, and MSE for $Q = LN$ approximately fixed, with $N = 1, 2, 4$ and $L = 81, 41, 21$ . (a) Coherent matched filters, averaged over Rayleigh channel realizations (channel model 1A). (b) Noncoherent matched filters with Rayleigh fading (channel model 3). MSEs are estimated from 4,000 runs . . . . .	33
6	Comparison of CRB, ZZB, and MSE for $Q = LN$ approximately fixed, with $N = 1, 2, 4$ and $L = 81, 41, 21$ . (a) Coherent matched filters, averaged over Rayleigh channel realizations. (b) Noncoherent matched filters with Rayleigh fading. MSEs are estimated from 6,000 runs . . . . .	33

---

## List of Tables

1	Relations between the MLEs, CRBs, and ZZBs for the five channel models . . . . .	15
---	--	----

INTENTIONALLY LEFT BLANK.

---

## 1. Introduction

---

Mobile ad hoc networks are highly desirable for military communication systems. The nodes in these networks frequently contain multiple antennas (giving rise to MIMO systems) and use frequency-hopping (FH) waveforms for low probability of intercept. In mobile ad hoc networks, time-delay estimation (TDE) is often used to estimate the locations of nodes in the network. Direct sequence or ultra-wideband waveforms are well-suited for TDE due to their large bandwidth. However, FH waveforms are desirable because they employ simpler receivers with large dynamic range and narrow bandwidth around each hopping frequency. The use of FH waveforms for TDE presents new challenges that require the analysis of the effects of fading and the diversity gained by integrating multiple hops, and we describe new results in this report.

The specific areas addressed in this report are as follows.

- a. Study source signal separation and channel estimation in MIMO communication systems when the signals are CM and training symbols are present. Investigate constrained Cramér-Rao (CRB) bounds, develop algorithms that jointly exploit the CM signal property and the training samples, and evaluate performance with computer simulations and experimentally measured data.
- b. Study TDE with FH communications waveforms. Evaluate tradeoffs in hop rate for fading channels, and analyze the value of training symbols and the impact of carrier uncertainty.
- c. Investigate the design of waveforms for quasi-synchronous superposition that maximize coherent gain, for potential use in cooperative transmission in ad hoc networks.

The report is organized as follows. Section 2 of this report contains a review of performance bounds for TDE, including a discussion of current trends. Sections 3 through 6 contain an analysis of TDE performance bounds and estimators for signals that are received on parallel, flat, Rayleigh fading channels. The model is applicable to FH waveforms, where the signals are orthogonal in time, as well as a sum-of-tones waveform in which the signals are orthogonal in frequency. The maximum-likelihood estimator (MLE), CRB, and Ziv-Zakai bound (ZZB) are presented for five models of the channel gain parameters: (1) known values, (2) unknown, deterministic parameters, (3) zero-mean, complex, Gaussian random variables (Rayleigh fading), and (1A), (2A) which are cases (1) and (2) averaged over the Rayleigh fading model in (3). Results from Monte Carlo simulations are presented that compare the mean-squared error (MSE) of the MLEs to the appropriate

bounds. The simulations indicate that the ZZB provides a significantly tighter bound than the CRB, and the ZZB exhibits a signal-to-noise ratio (SNR)-threshold region that agrees with the MSE performance of the MLE. The examples are restricted to a complex envelope signal model at baseband and Rayleigh fading. However, the analysis is general and may be applied to passband signals as well as Rician fading. In addition, the ZZB expressions may enable analytical characterization of the threshold performance of the MLE.

---

## 2. A Survey of Time Delay Estimation Performance Bounds

---

In this section we review performance bounds, as well as some current trends, in TDE. Research over several decades reveals that a few key parameters determine TDE performance. The most basic are the SNR, and the signal time-bandwidth (TB) product; larger values for each are desirable. The CRB reveals asymptotic MLE behavior with respect to TB and SNR. At moderate to lower SNR, TDEs generally break down as ambiguities arise due to increased noise and the cross-correlation of the signal, causing the TDE to deviate (often quite sharply) away from the CRB. Because it is a local bound, the CRB does not indicate the threshold behavior, and Ziv-Zakai and other bounds have been developed to handle this. When TD is measured between multiple sensors, the coherence between them can fundamentally limit the result, an effect that occurs in acoustics due to the turbulent atmosphere. We discuss modifications to the classical bounds that accommodate the coherence loss, and reveal a threshold coherence phenomenon. When communications and other signals are used for TDE, they may have significant nuisance parameters, including carrier uncertainty, unknown symbols, as well as effects due to an unknown channel. New TDE performance limits reveal the effect of these parameters for various signal models, including the impact of diversity channels on TDE, and this is considered beginning in section 3.

TDE is basic to many scenarios, being intimately linked to detection, array processing, surveillance, synchronization in communications, range finding in RADAR, as well as geolocation and tracking in sensor networks. Because of this, TDE has a long history. In this report, we survey TDE performance analysis results, with the caveat that such a large topic could fill many more pages, and many more papers could easily have been cited. While the topic is old, there continues to be progress and unsolved problems become important, particularly in the areas of sensor networking, networked geolocation, and communications. In addition to some now classical results, we also discuss some more recent problems and partial performance analysis solutions. In the rest of this introduction, we discuss the relevant parameters and issues associated with TDE performance.

When the signals are coherent (e.g., identical up to a delay on two or more sensors, or employing a single sensor when the signal is known to the receiver), CRB analysis on the delay parameter indicates that the performance is fundamentally limited by the signal TB product and the SNR, e.g., see Whalen (*53, 31*). The CRB on TDE is the subject of section 2.1. Thus, for stationary signals in a stationary channel, TDE performance is enhanced by longer duration, wider bandwidth, and higher energy or power signals. Of course, in most scenarios the TB, SNR, and coherence times are prescribed within some observable range, and the MLE of TD does not always achieve the performance predicted by the CRB.

The CRB provides a local bound on unbiased estimators based on the curvature of the likelihood around the true parameter value, but it does not account for large errors that occur with ambiguity-prone signals. For example, the TDE is often obtained from the peak of a correlation operation (this is the MLE in many scenarios). The correlation function is oscillatory for many signals of interest, so a neighboring peak may be selected incorrectly, leading to a large error in the TDE. The looseness of the CRB thus motivated a search for tighter bounds and a study of the conditions under which the MLE achieves the CRB. The study of tighter bounds that predict TDE threshold behavior is the subject of section 2.2. We focus on the Ziv-Zakai and Weiss-Weinstein bounds (WWBs). Generally, these bounds may incorporate a prior on the TD parameter, they bound the MSE and are not restricted to unbiased estimation, and are tighter than the associated CRB and subsume it. Finding these bounds is less of a turn-the-crank procedure than the CRB.

In some cases, the signals arriving at two or more sensors may be only partially coherent. This is the subject of section 2.3. This situation arises, for example, in aeroacoustics due to random fluctuations in the propagation medium. Although this effect has long been recognized (*30*), TDE performance effects have only recently been fully characterized, by extending Ziv-Zakai analysis to incorporate spatial coherence (*25*). Here, a threshold coherence effect is observed, such that for a given TB, the coherence must be above a threshold to obtain useful TDEs, independent of SNR. The model used here has connections to multiplicative noise models used in electromagnetic signal processing.

In communications, the impact of TDE is reflected in the acquisition and synchronization steps early in the receiver processing chain. It is also of interest to exploit communications devices and waveforms for TDE, for example, to perform geolocation in a network. This leads to the topic of TDE when diversity channels are available, and this is treated beginning in section 3.

## 2.1 Cramér-Rao Bound

**Deterministic signal model:** Many early TDE performance studies concentrated on the CRB. Consider the signal model

$$r(t) = s(t; \theta) + n(t), \quad 0 \leq t \leq T. \quad (1)$$

Here, the real-valued deterministic signal  $s(t)$  is known up to some parameters in  $\theta$ . The noise is assumed to be additive white Gaussian (AWGN), with two-sided power spectral density (PSD)  $N_o$ . The simplest case is  $s(t; \theta) = s(t - \tau)$ ,  $\theta = \tau$ , and it is assumed that the delay  $\tau$  is such that  $s(t; \theta)$  is completely contained in the interval  $[0, T]$ , with  $s(t)$  non-zero in  $[0, T_s]$ . This continuous time model ignores any sampling or quantization error that arises in a discrete-time version of equation 1.

The CRB is given by (e.g., see Helstrom and references therein (15))

$$\text{CRB}(\hat{\tau}) = \frac{1}{\text{SNR} \cdot \beta^2}. \quad (2)$$

with SNR and signal energy given by

$$\text{SNR} = \frac{E}{N_o}, \quad (3)$$

$$E = \int_0^{T_s} s^2(t) dt. \quad (4)$$

The factor  $\beta^2$  is the mean square bandwidth of  $s(t)$ , given by

$$\beta^2 = \frac{\int_0^{T_s} \left( \frac{ds(t)}{dt} \right)^2 dt}{\int_0^{T_s} s^2(t) dt} = \frac{\int_{-\infty}^{\infty} (2\pi f)^2 |S(f)|^2 df}{\int_{-\infty}^{\infty} |S(f)|^2 df}, \quad (5)$$

where  $S(f)$  is the Fourier transform of  $s(t)$ . For connection with the discrete-time case of equation 1, see (21). The CRB equation 2 is lowered by increasing the SNR, or increasing the signal bandwidth. The result is not strongly dependent on the particular shape of  $s(t)$ , but rather its overall energy and bandwidth.

For equation 1, the MLE results from maximizing the likelihood function. The TD MLE for this case is to choose the peak output of the matched filter, e.g., (15). More generally, when there are nuisance parameters, so that  $\theta$  is a vector including  $\tau$  and other unknowns, then the matched filter generalizes to a search over possible values for  $\theta$  in the correlation of the received signal with  $s(t; \theta)$ . For example, when the signal has unknown frequency shift, perhaps due to Doppler effects, then the resulting correlation is referred to as the ambiguity function.

The narrow band case of equation 1 allows us to write the signal as

$$s(t; \theta) = A \cdot \text{Re} \{ f(t - \tau) \exp(j\omega(t - \tau)) \}, \quad (6)$$

where  $f(t)$  is the complex envelope,  $\omega$  is the carrier frequency, and  $A$  is the amplitude. The problem of detection and time-delay estimation with equation 6 has been studied extensively in the context of radar and communications, e.g., see (15).

**Gaussian signal model:** When the signal model is not known precisely, an alternative is to assume it is random and Gaussian. This model has been studied extensively, e.g., in the context of acoustics, and many works in (6) address this case. With Gaussian signal and noise, second-order statistics are sufficient.

Consider the two-sensor case, given by

$$\begin{aligned} r_1(t) &= s(t) + n_1(t) \\ r_2(t) &= s(t - \tau) + n_2(t). \end{aligned} \quad (7)$$

Signal  $s(t)$  is a realization of a random Gaussian process, observed on an array, with independent AWGN on each element. Now, TDE corresponds to the delay observed between the sensors, so is sometimes referred to as time difference of arrival (TDOA) estimation. The signal is observed over a time interval of length  $T$ . This model allows us to fix the signal power spectrum while varying the observation time.

The CRB on TDE for this model is developed in Chow and Schultheiss (9), which we review for the case of two sensors.\* Let the PSDs of the signal and noise processes in equation 7 be denoted by  $S(\omega)$ ,  $N_1(\omega)$ ,  $N_2(\omega)$ . The Fisher information for TDE with large time-bandwidth product is, in general (6),

$$J_{CR}(\hat{\tau}) = \frac{T}{2\pi} \int_{-\infty}^{\infty} \omega^2 \text{SNR}(\omega) d\omega, \quad (8)$$

where  $\text{SNR}(\omega)$  is defined as

$$\text{SNR}(\omega) = \frac{(S(\omega)/N_1(\omega)) (S(\omega)/N_2(\omega))}{1 + (S(\omega)/N_1(\omega)) + (S(\omega)/N_2(\omega))} \quad (9)$$

and the CRB =  $J_{CR}^{-1}$ . Consider the case where the signal and noise PSDs are flat,

$$S(\omega) = \begin{cases} S, & |\omega| \in [\omega_c - B/2, \omega_c + B/2] \\ 0, & \text{otherwise} \end{cases}, \quad (10)$$

and  $N_1(\omega) = N_2(\omega) = N_o$ , where the center frequency is  $\omega_c$  and the bandwidth is  $B$  rad/sec. Then the SNR in equation 9 is

$$\text{SNR} = \frac{(S/N_o)^2}{1 + 2(S/N_o)} \quad (11)$$

---

\*A general expression with a linear array is given in (9).

and the Fisher information in equation 8 evaluates to

$$J_{CR}(\hat{\tau}) = 2\omega_c^2 \left(\frac{TB}{2\pi}\right) \left[1 + \frac{1}{12} \left(\frac{B}{\omega_c}\right)^2\right] \text{SNR}. \quad (12)$$

The analysis employs Fourier series, and  $T \gg 2\pi/B$  is needed to satisfy an assumption that the Fourier series coefficients are independent.<sup>†</sup> As the observation time doubles, the CRB shifts downward by 3 dB. Also, the CRB scales with the inverse of SNR  $S/N_o$  and with the inverse of center frequency  $\omega_c^2$ .

For this model equation 7, the MLE of  $\tau$  corresponds to choosing the peak output of the cross-correlation between  $r_1(t)$  and  $r_2(t)$ , e.g., see (14, 6), and references therein. This theory has been developed extensively (6), including estimators that account for intervening linear channels, leading to the so-called generalized cross-correlator (GCC). The GCC generally assumes known statistics, and is a weighted (non-parametric) cross-correlation TDE, e.g., see Hero and references therein (16). The case of unknown statistics was considered by Friedlander and Porat (11).

## 2.2 Ziv-Zakai and Weiss-Weinstein Bounds

The CRB predicts the MLE asymptotic performance, as a function of TB and/or SNR. However, it fails to predict the TDE behavior at more moderate values of these parameters. This threshold behavior arises from ambiguities that are particular to the signal and its correlation. For example, when TDEs arise from cross-correlation with narrow band signals, a neighboring peak may be incorrectly selected, leading to a large TDE error, e.g., see Ianniello (18).

Several approaches have been used to develop bounds tighter than the CRB. Chow and Schultheiss (9) considered this problem, employing the Barankin bound (BB), specifically, the Chapman-Robbins version of the BB. Ianniello investigated the problem by analyzing the probability of large errors (18, 39, 20). Ziv and Zakai developed an approach based on hypothesis testing (58), and various cases and improvements were subsequently derived (41, 8, 3, 4, 46).

The ZZBs have been found to be tighter than the BBs, and the ZZBs generally converge to the corresponding CRB, so that they subsume CRB analysis. The ZZB and its variants provide tight bounds for threshold behavior of TDEs, predicting when the MLE breaks down and departs from the CRB with good accuracy for many TDE scenarios. These bounds generally account for a priori limits on the time delay. The ZZBs are Bayesian bounds that treat the time delay as a random parameter, typically uniformly distributed on

---

<sup>†</sup>For this model, Gaussianity of the Fourier series coefficients follows immediately. For more general signal models, Gaussianity follows via a central limit theorem argument with large  $T$ .

an interval. In addition, the ZZBs bound MSE, and are not limited to unbiased estimates as is the CRB, which treats the time delay as a deterministic parameter. Given prior limits on  $\tau$ , it can be expected that estimators will be biased when  $\tau$  approaches the boundaries.

We review the ZZB beginning with the model in equation 7, with observation time  $T$ ,  $-T/2 \leq t \leq T/2$ . The signal and noise are assumed Gaussian, with spectral densities  $S(\omega)$ ,  $N_1(\omega)$ , and  $N_2(\omega)$ . The ZZB begins with a binary decision problem based on some arbitrary estimate  $\hat{\tau}$  of  $\tau$ ,

$$\begin{aligned} \text{Decide } H_0 : \tau = a & \quad \text{if } |\hat{\tau} - a| < |\hat{\tau} - a - \theta|, \\ \text{Decide } H_1 : \tau = a + \theta & \quad \text{if } |\hat{\tau} - a| > |\hat{\tau} - a - \theta|. \end{aligned} \quad (13)$$

Without loss of generality, the two hypothesized delays are considered to be equally likely, so the probability of error is  $P\{\hat{\tau} - a > \theta/2 | \tau = a\}/2 + P\{\hat{\tau} - a - \theta < -\theta/2 | \tau = a + \theta\}/2$ . Now, the error in estimating  $\tau$  by  $\hat{\tau}$  is  $\epsilon = \hat{\tau} - \tau$ .

We are interested in the mean square error  $\bar{\epsilon}^2 = E(\epsilon\epsilon^T)$  with  $\tau$  uniformly distributed within the interval  $[-D/2, D/2]$ , and  $\theta$  within  $[0, D]$ . The basic ZZB is given by (8)

$$\bar{\epsilon}^2 \geq \frac{1}{D} \int_0^D \theta \, d\theta \int_{-D/2}^{D/2-\theta} P_e(a, a + \theta) \, da, \quad (14)$$

where  $P_e(a, a + \theta)$  is the minimum attainable probability of error associated with the likelihood ratio test between the two hypothesized delays. It immediately follows that

$$P_e(a, a + \theta) \leq \frac{1}{2} \{P(\epsilon > \theta/2 | \tau = a) + P(\epsilon < -\theta/2 | \tau = a + \theta)\}. \quad (15)$$

An improvement is possible by noting that  $\int_{-D/2}^{D/2-\theta} P_e(a, a + \theta) da$  is a nonincreasing function of  $\theta$  (3). Therefore, by using a nonincreasing function  $\mathcal{V}[\cdot]$  that fills the valleys of the bracketed function, an improved ZZB is given by

$$\bar{\epsilon}^2 \geq \frac{1}{D} \int_0^D \theta \, \mathcal{V} \left[ \int_{-D/2}^{D/2-\theta} P_e(a, a + \theta) \, da \right] \, d\theta. \quad (16)$$

If  $P_e(a, a + \theta) = P_e(\theta)$ , so it is independent of  $a$ , then equation 16 may be simplified to (48)

$$\bar{\epsilon}^2 \geq \frac{1}{D} \int_0^D \theta \, \mathcal{V}[(D - \theta)P_e(\theta)] \, d\theta. \quad (17)$$

When the observation time  $T$  is large compared to the correlation time  $2\pi/B$  where  $B$  is the bandwidth, then  $P_e(\theta)$  is closely approximated by

$$P_e(\theta) \approx e^{a(\theta)+b(\theta)} \Phi(\sqrt{2b(\theta)}), \quad (18)$$

where

$$a(\theta) = -\frac{T}{2\pi} \int_0^\infty \ln[1 + \text{SNR}(\omega) \sin^2(\omega\theta/2)] d\omega, \quad (19)$$

$$b(\theta) = \frac{T}{2\pi} \int_0^\infty \frac{\text{SNR}(\omega) \sin^2(\omega\theta/2)}{1 + \text{SNR}(\omega) \sin^2(\omega\theta/2)} d\omega, \quad (20)$$

$\text{SNR}(\omega)$  is defined in equation 9, and

$$\Phi(x) = \frac{1}{\sqrt{2\pi}} \int_x^\infty e^{-\mu^2/2} d\mu. \quad (21)$$

The derivation of equation 18 assumes large  $TB$ . As noted earlier, this condition is common in TDE performance analysis, and is typically met in practical scenarios; poor estimates may result in practice if this condition is not satisfied.

The ZZB generally requires numerical evaluation to approximate the integrals in equation 19, 20, and 17. However, Weiss and Weinstein derived closed-form expressions for disjoint bound segments, separated by thresholds, for narrow band (48) and wideband (49) waveforms. For example, when the signal and noise PSDs are flat with  $S_1(\omega) = S_2(\omega)$  as in equation 10 and small fractional bandwidth  $B/\omega_c \ll 1$ , it is shown in (49) that the CRB is attainable only if the SNR in equation 11 exceeds a threshold value given by

$$\text{SNR}_{\text{th}} = \frac{6}{\pi^2 \left(\frac{TB}{2\pi}\right) \left(\frac{B}{\omega_c}\right)^2} \left[ \Phi^{-1} \left( \frac{1}{24} \left(\frac{B}{\omega_c}\right)^2 \right) \right]^2, \quad (22)$$

where  $\Phi^{-1}$  denotes the inverse of the function in equation 21. The SNR threshold in equation 22 is a decreasing function of  $TB$  and  $B/\omega_c$ . The closed-form ZZB expressions developed in (48, 49) are valuable for simplified analytical performance study when the fractional bandwidth is small or moderate. Simplified ZZB expressions for large fractional bandwidth (the ultra-wideband case) have also been developed (17). The ZZB in the above works is generally restricted to estimation of scalar random variables; it was extended to arbitrarily distributed, vector random variables by Bell et al. in (2).

Simulation examples comparing cross-correlation TDEs and the corresponding ZZBs show close agreement. For example, using realizations of Gaussian signals with flat-topped spectra, and given sufficient time-bandwidth ( $TB > 50$ , say), the ZZB accurately predicts threshold behavior for narrow band and wideband cases (19), as well as for ultra-wideband (17). These results suggest that, for equation 7, the cross-correlator is essentially optimal even in the non-asymptotic regime.

So far we have focused on the ZZB, which can be readily evaluated numerically, and approximations are available for some cases. Another bounding approach is available, due to Weiss and Weinstein, that is referred to as the WWB (44, 50, 51, 45). The WWB is a

family of MSE bounds on moments of random parameter estimators; the most general statement is in (45). Unfortunately, space limits our ability to give a full statement of the WWB. The WWB does not require regularity conditions, incorporates a priori distribution on the parameter, and is not restricted to unbiased estimates. Application of the WWB requires exploration of test points, and optimization over parameters in the bound, and this must be carried out for each case of interest. Simple expressions for the WWB for time delay have been derived for square pulses (50), and narrow band pulses with a trapezoidal envelope (51). Note that regularity is violated, e.g., with a square pulse, so that the CRB does not exist.

For the Gaussian case, the ZZB is readily evaluated numerically via the above equations, and, as we have noted, some specific cases have been developed for the ZZB and WWB. The ZZB and WWB provide significantly tighter performance bounds than the CRB, but also require more effort, whereas the CRB is more of a turn-the-crank analytical procedure. For both the ZZB and the WWB, it may be possible to find simplified expressions that are easily manipulated and provide valuable insight. The choice of test points is important for the WWB (and BB), and this can make evaluation of the bound significantly more complex as more parameters are added to the problem. The vector ZZB also faces a complexity increase due to the maximization needed (2). An interesting comparison of the ZZB and WWB for matched field processing with multiple parameters shows that, for this problem, the ZZB provides a somewhat better characterization of threshold behavior than does the WWB (57).

The WWB applies to vector parameters and functions of the parameters, and the WWB family was recently extended by Renaux et al., (36). Barankin bounds have been developed by Zeira and Schultheiss (55, 56) for active ranging systems with multiple echoes, and Schultheiss et al studied TDE in the non-Gaussian case in (40).

### 2.3 Impact of Coherence

The TDE model in equation 7 assumes that the random signal  $s(t)$  is identical at the two sensors. As mentioned above, the model has been extended to allow the signal components at the two sensors to differ by an unknown, deterministic, linear filtering operation, e.g., see (16) and references therein. However, in some scenarios, *random* phenomena in the propagation medium cause a loss in the *coherence* (i.e., correlation) between the signals that arrive at a pair of spatially separated sensors. In this section, we review the impact of signal coherence loss on TDE, and we present CRB and ZZB results that are explicitly parameterized by the signal coherence (25, 24). TDE performance is significantly impacted by imperfect signal coherence, and the ZZB analysis reveals that there exists a “threshold coherence” value that must be exceeded in order for TDE performance to achieve the CRB.

Signals propagating in many media undergo spatial coherence losses. In aeroacoustics (sounds propagating through air), signal coherence degrades with increased spatial separation between the sensors due to random scattering caused by atmospheric turbulence. Physics-based statistical models for the coherence as a function of frequency, range, weather conditions, and sensor separation are reviewed and applied to signal processing performance analyses in (54, 27, 38, 26, 28). Scattering and coherence losses occur in underwater acoustics, e.g., see (34) for an early analysis of the CRB on TDE with scattering, with more recent work in (5, 22) and elsewhere. In medical ultrasonics (sounds in the MHz range propagating through living tissues), the CRB on TDE has been analyzed for partially correlated speckle signals (43, 7). Spatial coherence losses occur with electromagnetic signals due to local scatterers near the transmitter, e.g., (35), and narrow band angle-of-arrival estimation with imperfect spatial coherence has been studied.

We extend the model in equation 7 as follows to study TDE with partial signal coherence (25):

$$\begin{aligned} r_1(t) &= s_1(t) + n_1(t) \\ r_2(t) &= s_2(t - \tau) + n_2(t), \end{aligned} \tag{23}$$

where  $s_1(t), s_2(t)$  are real-valued, continuous-time, zero-mean, jointly wide-sense stationary, Gaussian random processes with PSDs  $S_1(\omega), S_2(\omega)$  and cross-spectral density (CSD)  $S_{12}(\omega)$ . The AWGN processes  $n_1(t), n_2(t)$  have PSDs  $N_1(\omega), N_2(\omega)$ , and they are independent from each other and from  $s_1(t), s_2(t)$ . The magnitude-squared *coherence* function for the signals  $s_1(t), s_2(t)$  is

$$|\gamma_s(\omega)|^2 = \frac{|S_{12}(\omega)|^2}{S_1(\omega) S_2(\omega)} \leq 1. \tag{24}$$

Coherence magnitude = 1 corresponds to perfect correlation between the signal components at the sensors, so  $s_1(t)$  and  $s_2(t)$  are related by a linear filtering operation. Coherence magnitude < 1 models frequency-selective, random effects in the propagation paths from the source to the sensors. The CSD for the observations  $r_1(t), r_2(t)$  in equation 23 is

$$R_{12}(\omega) = S_{12}(\omega) \exp(j\omega\tau), \tag{25}$$

and the coherence for  $r_1(t), r_2(t)$  is defined analogously to equation 24 and may be expressed as

$$|\gamma_r(\omega)|^2 = \frac{|\gamma_s(\omega)|^2}{\left[1 + \left(\frac{S_1(\omega)}{N_1(\omega)}\right)^{-1}\right] \left[1 + \left(\frac{S_2(\omega)}{N_2(\omega)}\right)^{-1}\right]}. \tag{26}$$

TDE performance bounds (CRB and ZZB) are characterized by the following SNR-like quantity,

$$\text{SNR}(\omega) = \frac{|\gamma_r(\omega)|^2}{1 - |\gamma_r(\omega)|^2} \quad (27)$$

$$\begin{aligned} &= \left\{ \frac{1}{|\gamma_s(\omega)|^2} \left[ 1 + \left( \frac{S_1(\omega)}{N_1(\omega)} \right)^{-1} \right] \left[ 1 + \left( \frac{S_2(\omega)}{N_2(\omega)} \right)^{-1} \right] - 1 \right\}^{-1} \\ &< \frac{|\gamma_s(\omega)|^2}{1 - |\gamma_s(\omega)|^2}, \end{aligned} \quad (28)$$

which reduces to the SNR in equation 9 when  $|\gamma_s(\omega)| = 1$ . Note that signal coherence loss ( $|\gamma_s(\omega)| < 1$ ) severely limits the SNR quantity in equation 27, where the upper bound in equation 28 corresponds to large SNR per sensor,  $(S_1/N_1), (S_2/N_2) \rightarrow \infty$ .

The Fisher information for TDE with  $TB \gg 2\pi$  and partial signal coherence is obtained using equation 27 in equation 8. For the case in which the signal and noise PSDs are flat with  $S_1(\omega) = S_2(\omega)$  as in equation 10, we can use equation 28 to bound the CRB as

$$\text{CRB}(\hat{\tau}) > \frac{(1/|\gamma_s|^2) - 1}{2\omega_c^2 \left(\frac{TB}{2\pi}\right) \left[1 + \frac{1}{12} \left(\frac{B}{\omega_c}\right)^2\right]}. \quad (29)$$

Note that the CRB is limited by the signal coherence and is not improved by increased SNR per sensor,  $(S_1/N_1), (S_2/N_2)$ .

The general ZZB framework was reviewed in equations 13–21, and next we apply the ZZB to the passband case in which the signal and noise PSDs are flat with  $S_1(\omega) = S_2(\omega)$  as in equation 10,  $\gamma_s(\omega) = \gamma_s$ ,  $N_1(\omega) = N_2(\omega) = N_o$ , and the fractional bandwidth is small,  $B/\omega_c \ll 1$ . Then the SNR in equation 27 is

$$\text{SNR} = \left[ \frac{1}{|\gamma_s|^2} \left( 1 + \frac{1}{(S/N_o)} \right)^2 - 1 \right]^{-1}. \quad (30)$$

For perfectly coherent signals, the ZZB analysis in (49) shows that the CRB is attainable only if the SNR in equation 11 exceeds the threshold value in equation 22. The ZZB is extended to partially coherent signals (25) by using equation 30 in the inequality  $\text{SNR} \geq \text{SNR}_{\text{th}}$ , which combined with  $|\gamma_s|^2 \leq 1$  yields the following threshold values for  $S/N_o$  and coherence that must be exceeded for CRB attainability:

$$\frac{S}{N_o} \geq \frac{1}{\sqrt{1 + \frac{1}{\text{SNR}_{\text{th}}}} - 1} \quad (31)$$

$$|\gamma_s|^2 \geq \frac{\left(1 + \frac{1}{(S/N_o)}\right)^2}{1 + \frac{1}{\text{SNR}_{\text{th}}}} > \frac{1}{1 + \frac{1}{\text{SNR}_{\text{th}}}} \text{ as } \frac{S}{N_o} \rightarrow \infty. \quad (32)$$

Note that the threshold coherence value in equation 32 is a function of  $TB$  and fractional bandwidth ( $B/\omega_c$ ) through the formula for  $\text{SNR}_{\text{th}}$  in equation 22.

Figure 1a contains a plot of the threshold coherence in equation 32 as a function of the  $TB$  product for several values of fractional bandwidth ( $B/\omega_c$ ) with  $(S/N_o) \rightarrow \infty$ .<sup>‡</sup> Note from figure 1a that for threshold coherence values in the range from about 0.1 to 0.95, each doubling of the fractional bandwidth reduces the required  $TB$  by a factor of 10.

Figure 1b shows results from a simulation example comparing the root-mean-square (RMS) error of a cross-correlation TDE estimator with the CRB from equation 12 for several values of signal coherence,  $\gamma_s$ . The signals are Gaussian random processes with bandwidth  $B = 2\pi 30$  rad/s centered at  $\omega_c = 2\pi 100$  rad/s. The signal, noise, and coherence are flat over the frequency band, with  $S/N_o = 100$  (20 dB) and the observation time is  $T = 3$  s. The threshold coherence for this case is 0.41, from equations 32 and 22. Note in figure 1b that the simulated RMS error on TDE diverges sharply from the CRB very near to the threshold coherence value of 0.41, illustrating the accuracy of the threshold coherence in equation 32. Other examples of the threshold coherence effect for accurate TDE with measured aeroacoustic data are available in (25, 1).

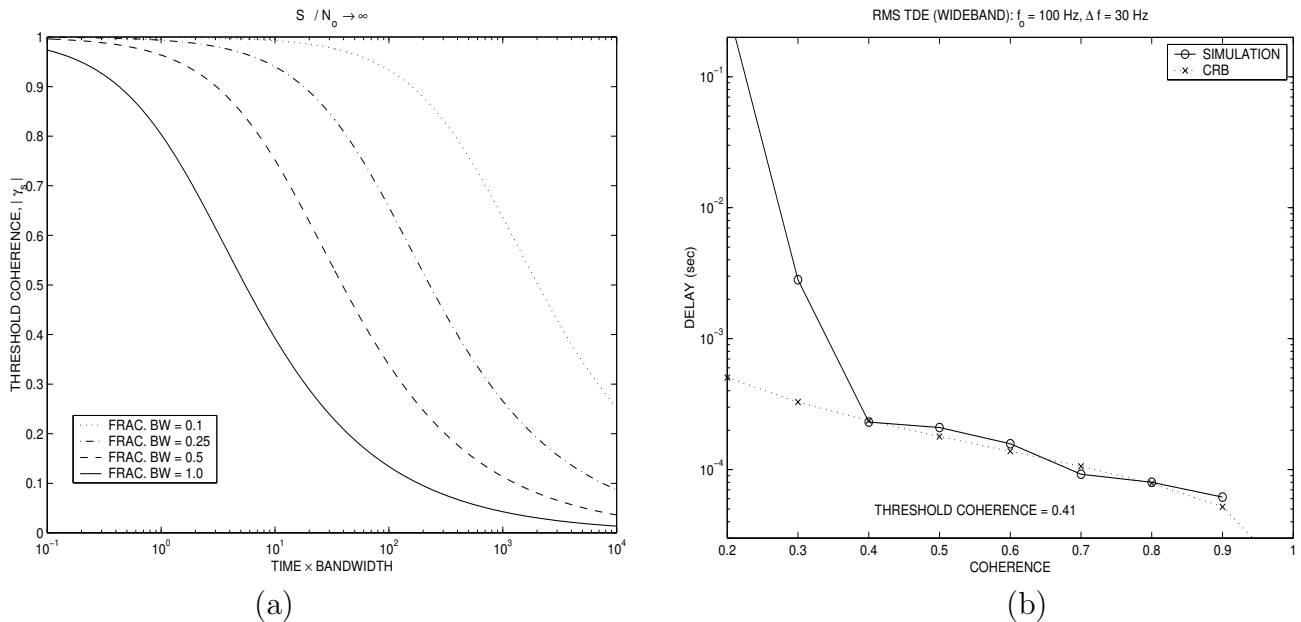


Figure 1. (a) Threshold coherence value from equation 32 versus time-bandwidth product  $TB$  for several values of fractional bandwidth  $B/\omega_c$  with  $S/N_o \rightarrow \infty$ . (b) Comparison of simulated RMS error for TDE with CRBs and threshold coherence value for signals with bandwidth  $B/(2\pi) = 30$  Hz centered at  $\omega_c/(2\pi) = 100$  Hz.

<sup>‡</sup>It is shown in (25) that the threshold coherence values are nearly equivalent for  $(S/N_o) > 10$  dB and  $(S/N_o) \rightarrow \infty$  when  $TB \gg 2\pi$ .

The generalized cross-correlator may be used for TDE with partial signal coherence,

$$\hat{\tau} = \arg \max_{\xi} \int_{-\infty}^{\infty} \hat{R}_{12}(\omega) G(\omega) \exp(j\omega\xi) d\omega, \quad (33)$$

where  $\hat{R}_{12}(\omega)$  is an estimate of the CSD in equation 25 and  $G(\omega)$  is a weighting function. The ML estimator uses weighting function  $G_{ML}(\omega) = \text{SNR}(\omega)/|R_{12}(\omega)|$ , while the the Wiener processor (16) may be more robust with  $G_{WP}(\omega) = |\gamma_r(\omega)|^2$ .

## 2.4 Sensor Networks and Geolocation

TDE has also received recent renewed interest in the context of sensor networks, as well as geolocation of mobile ad hoc network nodes. Many envisioned applications require node localization and/or tracking of position, and time delay estimates between nodes may be translated into accurate position estimates. This motivates the use of communications waveforms for TDE in wireless networks, e.g., see (33). Here, parametric models are applicable that incorporate nuisance parameters, such as carrier frequency and phase offsets, unknown symbols, and unknown channels. CRBs for TDE using these models are important in the study of synchronization for communications (42, 32). In the communications scenario, typically medium to high SNR is of interest, otherwise the SNR may be insufficient to provide a meaningful bit error rate. However, for TDE based geolocation, low SNR and threshold behavior is currently of interest (29).

---

## 3. TDE on Parallel, Flat Fading Channels

---

The remainder of this report presents an analysis of TDE performance bounds and estimators for signals that are received on parallel, flat, Rayleigh fading channels. The model is applicable to FH waveforms as in (29), where the signals are orthogonal in time, as well as a sum-of-tones waveform in which the signals are orthogonal in frequency. The MLE, CRB, and ZZB are presented for five models of the channel gain parameters: (1) known values, (2) unknown, deterministic parameters, (3) zero-mean, complex, Gaussian random variables (Rayleigh fading), and (1A), (2A) which are cases (1) and (2) averaged over the Rayleigh fading model in (3). We consider cases (1A) and (2A) because they are sometimes used when case (3) is intractable. However, in our model, all cases are tractable, allowing comparison of the various bounds. We present results from Monte Carlo simulations that compare the MSE of the MLEs to the appropriate bounds. The simulations indicate that the ZZB provides a significantly tighter bound than the CRB, and the ZZB exhibits a SNR-threshold region that agrees with the MSE performance of the MLE. The examples in this report are restricted to a complex envelope signal model at

baseband and Rayleigh fading. However, the analysis is general and may be applied to passband signals as well as Rician fading. In addition, the ZZB expressions may enable analytical characterization of the threshold performance of the MLE.

---

## 4. Signal Model

---

A general model for the complex envelope for TDE over  $N$  parallel channels is

$$r_i(t) = \gamma_i s_i(t - \tau) + n_i(t), \quad i = 1, \dots, N. \quad (34)$$

The  $s_i(t)$  are known waveforms,  $n_i(t)$  are complex, AWGN processes with zero mean and two-sided PSD  $\mathcal{N}_o$ , and each  $\gamma_i$  is a complex scalar representing the gain of the channel. We consider three models for the vector of complex channel gains,  $\boldsymbol{\gamma}$ .

- (1)  $\boldsymbol{\gamma}$  is known.
- (2)  $\boldsymbol{\gamma}$  is an unknown, deterministic, complex-valued parameter vector.
- (3) Each  $\gamma_i$  is a complex, circular, Gaussian random variable with zero mean and variance  $E\{|\gamma_i|^2\} = \sigma_s^2$ , independent for  $i = 1, \dots, N$ . This corresponds to Rayleigh fading that is independent from channel to channel, and is denoted by  $\boldsymbol{\gamma} \sim \text{CN}(\mathbf{0}, \sigma_s^2 \mathbf{I})$ . The average signal power,  $\sigma_s^2$ , is assumed known, and  $\mathbf{I}$  is the identity matrix.
- (1A) Case (1) averaged over the Rayleigh fading distribution, so  $\boldsymbol{\gamma} \sim \text{CN}(\mathbf{0}, \sigma_s^2 \mathbf{I})$ . This corresponds to a fading channel and a receiver that has a perfect estimate of  $\boldsymbol{\gamma}$ , so that the TDE is estimated with a coherent combination of the diversity channels.
- (2A) Case (2) averaged over the Rayleigh fading distribution, so  $\boldsymbol{\gamma} \sim \text{CN}(\mathbf{0}, \sigma_s^2 \mathbf{I})$ . This corresponds to (imperfect) estimation of  $\boldsymbol{\gamma}$  on each realization, and then averaging over the Rayleigh fading distribution.

Case 3 is different from case 2A in that  $\boldsymbol{\gamma}$  is not estimated in case 3 since it is modeled as a random vector. It is also possible to model the channel gain as  $\gamma_i = b_i \exp(j\theta_i)$  where  $b_i$  is an unknown, deterministic, positive parameter, and  $\theta_i$  is random with uniform distribution over  $[0, 2\pi)$  rad and independent for  $i = 1, \dots, N$ . The performance of this case is intermediate between cases 2 and 3, and we do not consider it here.

Our objective is to study the MLE, CRB, and ZZB on the time-delay parameter,  $\tau$  in equation 34, for the five channel model cases. The details are contained in the succeeding sections, but the results are summarized in table 1, from which we make the following observations.

Table 1. Relations between the MLEs, CRBs, and ZZBs for the five channel models.

	<i>Channel Model</i>				
	1	2	3	1A	2A
<b>MLE</b>	Coh MF	NonCoh MF	NonCoh MF	Coh MF	NonCoh MF
<b>CRB</b>	CRB <sub>1</sub>	CRB <sub>2</sub> = CRB <sub>1</sub>	CRB <sub>3</sub>	MCRB	ACRB = MCRB
<b>ZZB</b>	ZZB <sub>1</sub>	ZZB <sub>2</sub>	ZZB <sub>3</sub>	ZZB <sub>1A</sub>	ZZB <sub>2A</sub> = ZZB <sub>3</sub>

**Summary of channel model cases:**

- (1)  $\gamma$  is known.
- (2)  $\gamma$  is unknown, deterministic.
- (3) Rayleigh fading:  $\gamma \sim \text{CN}(\mathbf{0}, \sigma_s^2 \mathbf{I})$ .
- (1A) Case (1) averaged over  $\gamma \sim \text{CN}(\mathbf{0}, \sigma_s^2 \mathbf{I})$ .
- (2A) Case (2) averaged over  $\gamma \sim \text{CN}(\mathbf{0}, \sigma_s^2 \mathbf{I})$ .

- The MLE is a sum of *coherent* matched filters (MFs) in cases 1 and 1A, since  $\gamma$  is known. The MLE is a sum of *noncoherent* matched filters in cases 2, 3, and 2A. Although the MLEs are identical for several cases in table 1, the *performance* of the MLE varies from case to case, except that the performance is the same in cases 2A and 3.
- The CRBs for cases 1, 2, and 3 are generally distinct. However, for the known signal waveforms considered here that have even symmetry, the  $\tau$  and  $\gamma$  parameters are decoupled in the Fisher Information Matrix (FIM), so  $\text{CRB}_2 = \text{CRB}_1$ . The CRB is not defined for cases 1A and 2A, but the so-called modified CRB (MCRB) (13, 12) and asymptotic CRB (ACRB) (37) definitions are similar to these cases. We show that  $\text{CRB}_3 \rightarrow \text{ACRB} = \text{MCRB}$  at high SNR, and that the MCRB corresponds to  $\text{CRB}_1 = \text{CRB}_2$  when the fixed channel gains  $|\gamma_i|^2$  are replaced by the ensemble averages,  $E\{|\gamma_i|^2\} = \sigma_s^2$ .
- The ZZB is unique in four of the five channel model cases, and the ZZB is tractable in the four distinct cases.
- The five cases can be unified with a Rician fading model, and the ZZB is tractable for this case as well. This extension would be a useful item for future research.

When the model in equation 34 is applied with FH waveforms at baseband, then the complex envelope of the narrowband frequency hopping waveform in the  $i$ th hop is

$$s_i(t) = \sum_{k=-K}^K a_{k,i} h[t - (i-1)LT - kT], \quad i = 1, \dots, N, \quad (35)$$

where the pulse shape  $h(t)$  is real-valued and symmetric,  $T$  is the symbol duration,  $a_{k,i}$  is the  $k$ th symbol in the  $i$ th hop, and each hop has  $L = 2K + 1$  symbols and dwells for  $LT$  seconds. The symbols are assumed to be known and drawn from a constellation such as PSK with unit magnitude,  $|a_{k,i}| = 1$ . Over  $N$  hops, a total of  $Q = LN$  symbols are transmitted for a total signal duration of  $QT = LNT$  second. The pulse  $h(t)$  is a square-root, raised-cosine pulse with unit energy, so its autocorrelation is a Nyquist pulse:

$$\int_{-\infty}^{\infty} h(t) h(t + kT) dt = \delta_k, \quad (36)$$

where  $\delta_k$  is the Kronecker delta. When the model in equation 34 is applied to a sum-of-tones waveform, the signals in equation 34 have the form

$$s_i(t) = h(t) \exp(j\pi f_i t + \phi_i), \quad i = 1, \dots, N, \quad (37)$$

where  $h(t)$  is the pulse shape and  $f_i, \phi_i$  are the frequency and phase of the  $i$ th tone. In this report, results are developed as much as possible for an arbitrary signal shape  $s_i(t)$ , and then specialized to the baseband FH model in equation 35. The approach is applicable to the sum-of-tones model in equation 37, and it will be interesting to carry out the detailed analysis for this case in future work.

We conclude this section with a statement of the probability density function (pdf) for the model equation 34 for two cases: the conditional pdf,  $p_c(\mathbf{R} | \boldsymbol{\gamma}; \tau)$ , where  $\boldsymbol{\gamma}$  is a fixed vector, and the unconditional pdf,  $p_u(\mathbf{R} | \tau) = E_{\boldsymbol{\gamma}} \{p_c(\mathbf{R} | \boldsymbol{\gamma}; \tau)\}$ , that is averaged over  $\boldsymbol{\gamma} \sim \text{CN}(\mathbf{0}, \sigma_s^2 \mathbf{I})$ . The autocorrelation functions of the signals  $s_1(t), \dots, s_N(t)$  are defined as

$$\rho_i(\xi) = \int s_i(t - \xi)^* s_i(t) dt, \quad i = 1, \dots, N, \quad (38)$$

where  $*$  denotes complex conjugate and the limits on all integrals are  $(-\infty, \infty)$ . The coherent and noncoherent matched filters applied to channel  $i$  are defined as follows,

$$Y_i^{\text{COH}}(\xi) = \text{Re} \int \gamma_i^* s_i(t - \xi)^* r_i(t) dt \quad (39)$$

$$Y_i^{\text{NONCOH}}(\xi) = \left| \int s_i(t - \xi)^* r_i(t) dt \right|. \quad (40)$$

Let  $\mathbf{r}_i$  be a vector representation of  $r_i(t)$ , and define  $\mathbf{R} = [\mathbf{r}_1, \dots, \mathbf{r}_N]$ . Then the conditional pdf for  $\mathbf{R}$  has the following form, where factors independent of  $\boldsymbol{\gamma}, \tau$  are suppressed:

$$p_c(\mathbf{R} | \boldsymbol{\gamma}; \tau) \propto \prod_{i=1}^N \exp \left\{ \frac{1}{\mathcal{N}_o} [2 Y_i^{\text{COH}}(\tau) - |\gamma_i|^2 \rho_i(0)] \right\}. \quad (41)$$

The unconditional pdf is obtained by observing that  $\boldsymbol{\gamma} \sim \text{CN}(\mathbf{0}, \sigma_s^2 \mathbf{I})$  implies that  $\mathbf{r}_i \sim \text{CN}(\mathbf{0}, \boldsymbol{\Sigma}_i)$ , where the covariance matrix and inverse are

$$\boldsymbol{\Sigma}_i = \sigma_s^2 \mathbf{s}_i(\tau) \mathbf{s}_i(\tau)^H + \mathcal{N}_o \mathbf{I} \quad (42)$$

$$\boldsymbol{\Sigma}_i^{-1} = \frac{1}{\mathcal{N}_o} \left[ \mathbf{I} - \frac{\sigma_s^2 \mathbf{s}_i(\tau) \mathbf{s}_i(\tau)^H}{\mathcal{N}_o + \sigma_s^2 \rho_i(0)} \right], \quad (43)$$

where  $\mathbf{s}_i(\tau)$  is the vector representation of  $s_i(t - \tau)$  and  $^H$  is the conjugate-transpose operation. Then, ignoring terms and factors that are independent of  $\tau$ , the unconditional pdf is proportional to

$$p_u(\mathbf{R}|\tau) \propto \prod_{i=1}^N \exp \left\{ \frac{1}{\mathcal{N}_o} \cdot \frac{\sigma_s^2}{\mathcal{N}_o + \sigma_s^2 \rho_i(0)} \cdot Y_i^{\text{NONCOH}}(\tau)^2 \right\}. \quad (44)$$

We make the following assumptions:

1. The signal energy is the same on each channel,

$$\rho_i(0) = \int |s_i(t)|^2 dt \triangleq \rho(0), \quad i = 1, \dots, N. \quad (45)$$

Also, in order to simplify some of the formulas, we will assume that the signal autocorrelation functions in equation 38 are the same on each channel,

$$\rho_i(\xi) \triangleq \rho(\xi), \quad i = 1, \dots, N. \quad (46)$$

2. The signals have the property

$$\int s_i(t) \dot{s}_i(t)^* dt = 0, \quad i = 1, \dots, N, \quad (47)$$

where  $\dot{s}_i(t) \triangleq \frac{d}{dt} s_i(t)$ . This property holds for the sum-of-tones model in equation 37 as is approximately true for the FH model in equation 35, as will be shown in item 4 below.

3. The mean-squared signal bandwidth is the same on each channel and is denoted by  $B_s$  Hz, with definition

$$(2\pi B_s)^2 = \frac{1}{\rho(0)} \int |\dot{s}_i(t)|^2 dt = \frac{(2\pi)^2}{\rho(0)} \int f^2 |S_i(f)|^2 df. \quad (48)$$

where  $S_i(f)$  is the Fourier transform of  $s_i(t)$ .

4. For the FH model in equation 35, the symbols  $a_{k,i}$  are known and fixed, so the bounds (CRB and ZZB) are a function of the particular symbol sequence. However, the CRB and ZZB expressions are considerably simplified if we assume that time averages over the symbols are equal to the corresponding ensemble average for independent symbols drawn from the same constellation as the training sequence, i.e.,  $E\{a_{k,i} a_{l,i}^*\} = \delta_{kl}$ . Numerical evaluation shows that this approximation is very accurate even for training sequences as small as  $L = 10$  or  $20$ . For the FH model in equation 35, this leads to the following approximations that are used in the CRB and

ZZB expressions in the following section. First we define the autocorrelation function of the (real-valued) pulse shape,

$$\rho_h(\xi) = \int h(t - \xi) h(t) dt \quad (49)$$

$$= \text{sinc} \left( \frac{t}{T} \right) \frac{\cos(\pi\alpha t/T)}{1 - (2\alpha t/T)^2}. \quad (50)$$

where equation 50 is the raised-cosine pulse with excess bandwidth (or rolloff factor)  $\alpha \in [0, 1]$ , which is the result when  $h(t)$  is a square-root, raised-cosine pulse. Note that  $\rho_h(0) = 1$ . Then the signal autocorrelation functions in equation 38 have the form

$$\begin{aligned} \rho_i(\xi) &= L \rho_h(\xi) + \sum_{k \neq l} a_{k,i} a_{l,i}^* \rho_h(\xi + (l - k)T) \\ &\approx L \rho_h(\xi), \quad i = 1, \dots, N. \end{aligned} \quad (51)$$

Equation 47 has the form

$$\int s_i(t) \dot{s}_i(t)^* dt = L \int h(t) \dot{h}(t) dt + \sum_{k \neq l} a_{k,i} a_{l,i}^* \int h(t - kT) \dot{h}(t - lT) dt \quad (52)$$

$$\approx 0, \quad i = 1, \dots, N, \quad (53)$$

where the first term in equation 52 is zero due to the even and odd symmetry of  $h(t)$  and  $\dot{h}(t)$ , respectively, and the second term is approximately zero due to approximating the time average over the symbols by the ensemble average  $E\{a_{k,i} a_{l,i}^*\} = \delta_{kl}$ . The signal bandwidth in equation 48 has the form

$$\begin{aligned} \int |\dot{s}_i(t)|^2 dt &= \rho(0) (2\pi B_s)^2 \\ &= L \int \left| \dot{h}(t) \right|^2 dt + \sum_{k \neq l} a_{k,i} a_{l,i}^* \int \dot{h}(t - kT) \dot{h}(t - lT) dt \\ &\approx L (2\pi B_h)^2, \quad i = 1, \dots, N, \end{aligned} \quad (54)$$

where  $B_h$  Hz is the mean-squared bandwidth of the pulse  $h(t)$ . Note that  $\rho(0) = L$ , so the signals  $s_i(t)$  have the same bandwidth as the pulse  $h(t)$ , as expected for linear modulation. When  $h(t)$  is the square-root, raised-cosine pulse with excess bandwidth (or rolloff factor)  $\alpha \in [0, 1]$ , the mean-squared bandwidth  $B_h$  is (13)

$$B_h^2 = \frac{1}{T^2} \frac{1}{12} \left[ 1 + \alpha^2 \left( 3 - \frac{24}{\pi^2} \right) \right]. \quad (55)$$

Assumption 1 that the signal energy is the same on each channel in equation 45 implies that the log-likelihood (LL) functions for the conditional and unconditional cases are,

respectively,

$$\mathcal{L}_c(\mathbf{R}|\boldsymbol{\gamma};\tau) = \frac{1}{\mathcal{N}_o} \sum_{i=1}^N [2Y_i^{\text{COH}}(\tau) - |\gamma_i|^2 \rho(0)] \quad (56)$$

$$\mathcal{L}_u(\mathbf{R}|\tau) = \frac{1}{\mathcal{N}_o} \cdot \frac{\sigma_s^2}{\mathcal{N}_o + \sigma_s^2 \rho(0)} \sum_{i=1}^N Y_i^{\text{NONCOH}}(\tau)^2. \quad (57)$$

These LL functions are used in the next section to derive the MLEs, CRBs, and ZZBs for the various channel models.

---

## 5. TDE Estimators and Bounds

---

In this section, the MLEs, CRBs, and ZZBs are presented for the five channel models summarized in table 1.

### 5.1 Maximum Likelihood Estimators

We begin with the MLEs, and we define the sums of coherent and noncoherent matched filters as follows,

$$Z^{\text{COH}}(\xi) = \sum_{i=1}^N \text{Re} \left( \int \gamma_i^* s_i(t - \xi)^* r_i(t) dt \right) = \sum_{i=1}^N Y_i^{\text{COH}}(\tau) \quad (58)$$

$$Z^{\text{NONCOH}}(\xi) = \sum_{i=1}^N \left| \int s_i(t - \xi)^* r_i(t) dt \right|^2 = \sum_{i=1}^N Y_i^{\text{NONCOH}}(\tau)^2. \quad (59)$$

For case 1, the MLE is the value of  $\tau$  that maximizes the LL in equation 56 when  $\boldsymbol{\gamma}$  is known. The second term in equation 56 is independent of  $\tau$ , so the MLE for case 1 is the value that maximizes the sum of coherent matched filters,

$$\hat{\tau}_1 = \arg \max_{\xi} Z^{\text{COH}}(\xi). \quad (60)$$

For case 2,  $\boldsymbol{\gamma}$  is an unknown, deterministic parameter, so the MLE requires the joint maximization of the LL in equation 56 with respect to  $\tau$  and  $\boldsymbol{\gamma}$ . For a given TDE estimate  $\hat{\tau}$ , the MLE of each  $\gamma_i$  is

$$\hat{\gamma}_i = \frac{1}{\rho(0)} \int s_i(t - \hat{\tau})^* r_i(t) dt, \quad i = 1, \dots, N. \quad (61)$$

The estimates  $\hat{\gamma}_i$  in equation 61 are substituted for  $\gamma$  in the LL of equation 56, yielding the MLE for  $\tau$  in case 2 as the value that maximizes the sum of noncoherent matched filters,

$$\hat{\tau}_2 = \arg \max_{\xi} Z^{\text{NONCOH}}(\xi). \quad (62)$$

For case 3,  $\gamma \sim \text{CN}(\mathbf{0}, \sigma_s^2 \mathbf{I})$  so the MLE for  $\tau$  is the value that maximizes the unconditional LL in equation 57, which is identical to equation 62:

$$\hat{\tau}_3 = \arg \max_{\xi} Z^{\text{NONCOH}}(\xi). \quad (63)$$

For cases 1A and 2A, the MLEs are given by  $\hat{\tau}_1$  in equation 60 and  $\hat{\tau}_2$  in equation 62, respectively. The MLE performance is different in cases 1A and 2A (compared with cases 1 and 2 in which  $\gamma$  is fixed) due to averaging over realizations of values for  $\gamma \sim \text{CN}(\mathbf{0}, \sigma_s^2 \mathbf{I})$ . The MLEs are summarized in table 1, where ‘‘Coh MF’’ refers to equation 58 and ‘‘NonCoh MF’’ refers to equation 59.

## 5.2 Cramér-Rao Bounds

Next we consider the CRB. In general, let us denote the deterministic parameters by the vector  $\Theta$  and the LL function by  $\mathcal{L}(\mathbf{R} | \Theta)$ . Then the FIM,  $\mathbf{J}$ , has elements for parameters  $\theta_n \in \Theta$  given by

$$[\mathbf{J}(\Theta)]_{m,n} = E_{\mathbf{R}} \left\{ \frac{-\partial^2}{\partial \theta_m \partial \theta_n} \mathcal{L}(\mathbf{R} | \Theta) \right\}. \quad (64)$$

The CRB on  $\theta_n$  is the  $n$ th diagonal element in the inverse of the FIM,  $\text{CRB}(\theta_n) = [\mathbf{J}^{-1}]_{n,n}$ .

For cases 1, 2, and 3,  $\mathbf{r}_i$  is a complex, Gaussian random vector,  $\mathbf{r}_i \sim \text{CN}(\boldsymbol{\mu}_i, \mathbf{C}_i)$ , independent for  $i = 1, \dots, N$ , for which the FIM elements are given by (21)

$$[\mathbf{J}(\Theta)]_{m,n} = \sum_{i=1}^N \left\{ \text{tr} \left[ \mathbf{C}_i^{-1} \frac{\partial \mathbf{C}_i}{\partial \theta_m} \mathbf{C}_i^{-1} \frac{\partial \mathbf{C}_i}{\partial \theta_n} \right] + 2 \cdot \text{Re} \left[ \frac{\partial \boldsymbol{\mu}_i^H}{\partial \theta_m} \mathbf{C}_i^{-1} \frac{\partial \boldsymbol{\mu}_i}{\partial \theta_n} \right] \right\}, \quad (65)$$

where  $\text{tr}(\cdot)$  denotes the trace of a matrix. For cases 1 and 2,  $\boldsymbol{\mu}_i = \gamma_i \mathbf{s}_i(\tau)$  and  $\mathbf{C}_i = \mathcal{N}_o \mathbf{I}$ , with  $\Theta = [\tau]$  for case 1 and  $\Theta = [\text{Re}(\gamma), \text{Im}(\gamma), \tau]$  for case 2. For case 3,  $\boldsymbol{\mu}_i = \mathbf{0}$  and  $\mathbf{C}_i = \boldsymbol{\Sigma}_i$  in (42), with  $\Theta = [\tau]$ .

The CRB for cases 1 and 2 can be obtained from the following FIM for case 2,

$$\mathbf{J}_2 \left( \begin{bmatrix} \text{Re}(\gamma) \\ \text{Im}(\gamma) \\ \tau \end{bmatrix} \right) = \frac{2}{\mathcal{N}_o} \begin{bmatrix} \rho(0) \mathbf{I}_{N \times N} & \mathbf{0} & \mathbf{0} \\ \mathbf{0} & \rho(0) \mathbf{I}_{N \times N} & \mathbf{0} \\ \mathbf{0} & \mathbf{0} & \rho(0) (2\pi B_s)^2 \sum_{i=1}^N |\gamma_i|^2 \end{bmatrix}, \quad (66)$$

where assumptions 1, 2, and 3 in equations 45, 47, and 48 have been used. The block-diagonal structure of equation 66 implies that the parameters  $\boldsymbol{\gamma}, \tau$  are decoupled in the FIM, so the CRBs for  $\tau$  are identical for cases 1 and 2,

$$\text{CRB}_1(\hat{\tau} | \boldsymbol{\gamma}) = \frac{1}{[\mathbf{J}_2]_{2N+1, 2N+1}} = \frac{\mathcal{N}_o}{2 (2\pi B_s)^2 \rho(0) \sum_{i=1}^N |\gamma_i|^2}. \quad (67)$$

$$\text{CRB}_2(\hat{\tau} | \boldsymbol{\gamma}) = \frac{1}{[(\mathbf{J}_2)^{-1}]_{2N+1, 2N+1}} = \frac{\mathcal{N}_o}{2 (2\pi B_s)^2 \rho(0) \sum_{i=1}^N |\gamma_i|^2}. \quad (68)$$

The notation on the left side of equations 67 and 68 is used to emphasize that the CRBs depend on the particular values of the channel gains,  $\boldsymbol{\gamma}$ . The FIM for case 3 is obtained from equation 65 with  $\boldsymbol{\mu}_i = \mathbf{0}$ ,  $\mathbf{C}_i = \boldsymbol{\Sigma}_i$  in equation 42, and  $\boldsymbol{\Theta} = [\tau]$ . Using assumptions 1, 2, and 3 in equations 45, 47, and 48, the CRB for case 3 can be expressed as

$$\text{CRB}_3(\hat{\tau}) = \frac{1 + \rho(0) (\sigma_s^2 / \mathcal{N}_o)}{2 (2\pi B_s)^2 N [\rho(0) \sigma_s^2 / \mathcal{N}_o]^2}. \quad (69)$$

The CRB in equation 69 is the “true” CRB for the Rayleigh fading channel model. The derivation of equation 69 is tractable, but it requires significantly more computation than the CRBs in equations 67 and 68 in which  $\boldsymbol{\gamma}$  is a deterministic parameter. A number of bounds that are looser than the CRB have been studied for models with random nuisance parameters, such as the MCRB, hybrid CRB (HCRB), ACRB, and the Extended Miller-Chang Bound (EMCB) (13, 12, 37). All of these bounds begin with a FIM in which  $\boldsymbol{\gamma}$  is modeled as a deterministic parameter, and then an averaging operation is performed over  $\boldsymbol{\gamma}$  on some function of the FIM. The CRB is not defined for channel models 1A and 2A in table 1 (case 3 provides the “true” CRB for Rayleigh fading), but the MCRB and ACRB are closely related to cases 1A and 2A, respectively. The MCRB is similar to our channel model 1A, where the FIM element in the denominator of equation 67 corresponding to known  $\boldsymbol{\gamma}$  is averaged (12), yielding

$$\text{CRB}_{1A}(\hat{\tau}) \approx \text{MCRB}(\hat{\tau}) \triangleq \frac{1}{E_{\boldsymbol{\gamma}} \left\{ [\mathbf{J}_2]_{2N+1, 2N+1} \right\}} = \frac{\mathcal{N}_o}{2 (2\pi B_s)^2 \rho(0) N \sigma_s^2}. \quad (70)$$

The ACRB (37) is similar to our channel model 2A, where the quantity in the denominator of equation 68 corresponding to unknown, deterministic  $\boldsymbol{\gamma}$  is averaged, yielding

$$\text{CRB}_{2A}(\hat{\tau}) \approx \text{ACRB}(\hat{\tau}) \triangleq \frac{1}{E_{\boldsymbol{\gamma}} \left\{ [(\mathbf{J}_2)^{-1}]_{2N+1, 2N+1} \right\}} = \frac{\mathcal{N}_o}{2 (2\pi B_s)^2 \rho(0) N \sigma_s^2}. \quad (71)$$

It is shown in (12) that the ACRB is a lower bound on the EMCB via Jensen’s inequality. Note from equations 69, 70, and 71 that the MCRB = ACRB are looser than the “true” CRB for Rayleigh fading in equation 69, and that the three bounds coincide at high SNR:

$$\text{CRB}_3(\hat{\tau}) \geq \text{MCRB}(\hat{\tau}) = \text{ACRB}(\hat{\tau}) \quad (72)$$

$$\text{CRB}_3(\hat{\tau}) \xrightarrow[\mathcal{N}_o \rightarrow \infty]{\sigma_s^2} \text{MCRB}(\hat{\tau}) = \text{ACRB}(\hat{\tau}). \quad (73)$$

The CRB results are specialized to the baseband FH signal model in equation 35 as follows. For channel model cases 1 and 2, the (deterministic) mean SNR per symbol over the  $N$  channels is

$$\text{SNR}_{\text{det}}(\boldsymbol{\gamma}) = \frac{1}{N} \sum_{i=1}^N \frac{|\gamma_i|^2}{\mathcal{N}_o}, \quad (74)$$

and for cases 1A, 2A, and 3 (Rayleigh fading), the mean SNR per symbol is defined as

$$\overline{\text{SNR}} = \frac{E\{|\gamma_i|^2\}}{\mathcal{N}_o} = \frac{\sigma_s^2}{\mathcal{N}_o} = E_{\boldsymbol{\gamma}}\{\text{SNR}_{\text{det}}(\boldsymbol{\gamma})\}. \quad (75)$$

Then using  $\rho(0) = L$  from equations 45 and 51,  $B_s = B_h$  from equation 54, and the SNR per symbol definitions in equations 74 and 75, the CRBs in equations 67–71 are as follows for the FH signal model,

$$\text{CRB}_1(\hat{\tau} | \boldsymbol{\gamma}) = \text{CRB}_2(\hat{\tau} | \boldsymbol{\gamma}) = [2 (2\pi B_h)^2 N \cdot L \cdot \text{SNR}_{\text{det}}(\boldsymbol{\gamma})]^{-1} \quad (76)$$

$$\text{CRB}_3(\hat{\tau}) = \left[ 2 (2\pi B_h)^2 N \frac{(L \cdot \overline{\text{SNR}})^2}{1 + L \cdot \overline{\text{SNR}}} \right]^{-1} \quad (77)$$

$$\text{CRB}_{1A}(\hat{\tau}) \approx \text{MCRB}(\hat{\tau}) = [2 (2\pi B_h)^2 N \cdot L \cdot \overline{\text{SNR}}]^{-1} \quad (78)$$

$$\text{CRB}_{2A}(\hat{\tau}) \approx \text{ACRB}(\hat{\tau}) = [2 (2\pi B_h)^2 N \cdot L \cdot \overline{\text{SNR}}]^{-1}. \quad (79)$$

We observe the following from the CRB analysis.

- The time delay  $\tau$  and channel gains  $\boldsymbol{\gamma}$  are decoupled in the FIM, so the CRBs are identical in cases 1 and 2 where the channel gains are modeled as known and unknown deterministic parameters, respectively.
- The MCRB and ACRB for channel model cases 1A and 2A are identical to  $\text{CRB}_1 = \text{CRB}_2$  without fading, as long as  $\text{SNR}_{\text{det}} = \overline{\text{SNR}}$ . Furthermore, the true  $\text{CRB}_3$  for Rayleigh fading coincides with the other CRBs at high SNR. Therefore the CRB is not very sensitive to the model for the channel gain parameters, particularly at high SNR.
- The CRBs are inversely proportional to the SNR, the pulse bandwidth  $B_h$ , and the total number of symbols,  $Q = L \cdot N$ , where  $N$  is the number of hops and  $L$  is the number of symbols per hop. The only exception is  $\text{CRB}_3$  in equation 77, which for fixed  $Q = LN$  and low SNR is minimized by  $N = 1$  hop. The other CRBs, as well as  $\text{CRB}_3$  at high SNR, depend only on the total number of symbols, so the CRB does not reveal a diversity advantage when more hops are used with fewer symbols per hop.

We will show in the following subsection that the Ziv-Zakai bounds are quite sensitive to the channel model, and that when the channel gains are random variables (fading), then

greater diversity (larger  $N$ ) provides significant improvement in the threshold SNR at which the MLE performance is equal to the CRB. The ZZBs indicate that with fading channels, the CRB on TDE is a tight bound only when there is sufficient diversity ( $N > 1$ ) and the SNR exceeds a threshold value.

### 5.3 Ziv-Zakai Bounds

The four distinct ZZBs summarized in table 1 are developed in this section using the expressions in equations 13–17. The general hypothesis test in equation 13 is stated as follows for the model of TDE over  $N$  parallel channels in equation 34:

$$H_0 : r_i(t) = \gamma_i s_i(t - a) + n_i(t), \quad i = 1, \dots, N \quad (80)$$

$$H_1 : r_i(t) = \gamma_i s_i(t - (a + \theta)) + n_i(t), \quad i = 1, \dots, N. \quad (81)$$

The hypotheses are modeled as equally likely. In the ZZB formulation,  $\tau$  is modeled as a uniform random variable on the interval  $[-D/2, D/2]$ , which represents *a priori* knowledge about the range of possible values for the time delay parameter,  $\tau$ . Therefore in equations 80 and 81,  $\theta > 0$  and  $a, (a + \theta) \in [-D/2, D/2]$ . Let  $P_e(a, a + \theta)$  denote the minimum probability of error in deciding between  $H_0$  and  $H_1$  for particular values of  $a, a + \theta$ . The  $P_e(a, a + \theta)$  is derived from a likelihood ratio test (LRT), so it depends on the model for the channel gain vector,  $\gamma$ . The conditional LL in equation 56 is used to find  $P_e$  for channel models 1 and 1A, with  $\gamma$  fixed in case 1 and averaged over  $\gamma$  in case 1A. For case 2, a generalized LRT (GLRT) formed with ML estimates of the channel gain parameters in equation 61 substituted into equation 56 reduces to a LRT based on equation 57, with  $\gamma$  fixed. Case 2A includes subsequent averaging over  $\gamma$ . The  $P_e$  for case 3 is based on the unconditional LL in equation 57, and is found to be identical to case 2A. This summarizes the procedure used to derive the four ZZBs in table 1, and the details are presented next.

For case 1, an error occurs in the LRT based on equation 56 in the following cases:

$$\text{If } H_0 \text{ is true: } \sum_{i=1}^N Y_i^{\text{COH}}(a) < \sum_{i=1}^N Y_i^{\text{COH}}(a + \theta) \quad (82)$$

$$\text{If } H_1 \text{ is true: } \sum_{i=1}^N Y_i^{\text{COH}}(a) > \sum_{i=1}^N Y_i^{\text{COH}}(a + \theta) \quad (83)$$

where  $Y_i^{\text{COH}}(\xi)$  is defined in equation 39. The minimum probability of error for case 1,  $P_{e,1}(a, a + \theta | \gamma)$ , is one-half the probability of equation 82 plus one-half the probability of equation 83. It is straightforward to show that equations 82 and 83 have equal probability that is independent of  $a$ , so for case 1 with  $\gamma$  known and  $a = 0$ ,

$$P_{e,1}(\theta | \gamma) = \Pr \left\{ \sum_{i=1}^N [Y_i^{\text{COH}}(0) - Y_i^{\text{COH}}(\theta)] < 0 \mid H_0 \right\}. \quad (84)$$

The result for case 1A is obtained by averaging over  $\boldsymbol{\gamma}$ ,

$$P_{e,1A}(\theta) = E \{P_{e,1}(\theta | \boldsymbol{\gamma})\}. \quad (85)$$

For case 2, the hypothesis test equations 80 and 81 contains the unknown, deterministic channel gain parameters,  $\boldsymbol{\gamma}$ . The GLRT is formed by substituting the ML estimates of the channel gain parameters in equation 61 into equation 56, which by equation 62 results in LL functions that are a sum of noncoherent matched filters, as in equation 57. As in case 1, the error has equal probability under  $H_0$  and  $H_1$  and is independent of  $a$ , so with  $a = 0$

$$P_{e,2}(\theta | \boldsymbol{\gamma}) = \Pr \left\{ \sum_{i=1}^N [Y_i^{\text{NONCOH}}(0)^2 - Y_i^{\text{NONCOH}}(\theta)^2] < 0 \mid H_0 \right\}, \quad (86)$$

where  $Y_i^{\text{NONCOH}}(\xi)$  is defined in equation 40. The result for case 2A is obtained by averaging over  $\boldsymbol{\gamma}$ ,

$$P_{e,2A}(\theta) = E \{P_{e,2}(\theta | \boldsymbol{\gamma})\}. \quad (87)$$

For case 3, the LRT is based on equation 57, the error has equal probability under  $H_0$  and  $H_1$  and is independent of  $a$ , so with  $a = 0$

$$P_{e,3}(\theta) = \Pr \left\{ \sum_{i=1}^N [Y_i^{\text{NONCOH}}(0)^2 - Y_i^{\text{NONCOH}}(\theta)^2] < 0 \mid H_0 \right\} \quad (88)$$

$$= P_{e,2A}(\theta). \quad (89)$$

The probability in equation 88 is computed with respect to the additive noise and  $\boldsymbol{\gamma} \sim \text{CN}(\mathbf{0}, \sigma_s^2 \mathbf{I})$ , so the result is identical to case 2A, as indicated by equation 89. Next, we provide expressions for the probabilities in equations 84–86, and 88. The ZZB for each case is obtained by using the corresponding  $P_e$  in equation 17, which is repeated here for convenience,

$$\text{ZZB}(\hat{\tau}) \geq \frac{1}{D} \int_0^D \theta \mathcal{V}[(D - \theta)P_e(\theta)] d\theta, \quad (90)$$

where  $\mathcal{V}[\cdot]$  is a nonincreasing function that fills the valleys of the bracketed function,

We begin with case 1 and the evaluation of equation 84, where

$$U_i \triangleq Y_i^{\text{COH}}(0) | H_0 = \text{Re} \int \gamma_i^* s_i(t)^* [\gamma_i s_i(t) + n_i(t)] dt \quad (91)$$

$$= |\gamma_i|^2 \rho(0) + \text{Re} \left[ \underbrace{\gamma_i^* \int s_i(t)^* n_i(t) dt}_{A_i} \right] \quad (92)$$

$$V_i \triangleq Y_i^{\text{COH}}(\theta) | H_0 = \text{Re} \int \gamma_i^* s_i(t - \theta)^* [\gamma_i s_i(t) + n_i(t)] dt \quad (93)$$

$$= |\gamma_i|^2 \text{Re} [\rho_i(\theta)] + \text{Re} \left[ \underbrace{\gamma_i^* \int s_i(t - \theta)^* n_i(t) dt}_{B_i} \right] \quad (94)$$

The  $A_i$ ,  $B_i$  are complex, circular, correlated, Gaussian random variables with zero mean and

$$E \{|A_i|^2\} = \rho(0) \mathcal{N}_o \quad (95)$$

$$E \{|B_i|^2\} = \rho(0) \mathcal{N}_o \quad (96)$$

$$E \{A_i B_i^*\} = \rho_i(-\theta) \mathcal{N}_o \quad (97)$$

$$\begin{bmatrix} A_i \\ B_i \end{bmatrix} \sim \text{CN} \left( \mathbf{0}, \rho(0) \mathcal{N}_o \begin{bmatrix} 1 & \rho_i(\theta)^*/\rho(0) \\ \rho_i(\theta)/\rho(0) & 1 \end{bmatrix} \right). \quad (98)$$

It follows that the second terms in equations 92 and 94 are real-valued, correlated, Gaussian random variables with zero mean and covariance matrix

$$\begin{bmatrix} \text{Re} [\gamma_i^* A_i] \\ \text{Re} [\gamma_i^* B_i] \end{bmatrix} \sim \text{N} \left( \mathbf{0}, \frac{1}{2} |\gamma_i|^2 \rho(0) \mathcal{N}_o \begin{bmatrix} 1 & \text{Re} [\rho_i(\theta)]/\rho(0) \\ \text{Re} [\rho_i(\theta)]/\rho(0) & 1 \end{bmatrix} \right), \quad (99)$$

and the random vectors in equation 99 are independent for  $i = 1, 2, \dots, N$ . The minimum probability of error for case 1 in equation 84 is then

$$P_{e,1}(\theta | \gamma) = \Pr \left\{ \sum_{i=1}^N [U_i - V_i] < 0 | H_0 \right\}. \quad (100)$$

Using equations 92, 94, and 99, the independence over  $i$ , and the assumption  $\rho_i(\xi) = \rho(\xi)$  in equation 46,

$$\sum_{i=1}^N [U_i - V_i] \sim \text{N} \left( (\rho(0) - \text{Re}[\rho(\theta)]) \sum_{i=1}^N |\gamma_i|^2, (\rho(0) - \text{Re}[\rho(\theta)]) \mathcal{N}_o \sum_{i=1}^N |\gamma_i|^2 \right), \quad (101)$$

so equation 100 is expressed as

$$P_{e,1}(\theta | \gamma) = Q \left( \sqrt{\rho(0) \cdot N \cdot \text{SNR}_{\text{det}}(\gamma) \cdot (1 - \text{Re}[\rho(\theta)]/\rho(0))} \right) \quad (102)$$

where

$$Q(y) = \frac{1}{\sqrt{2\pi}} \int_y^\infty \exp(-u^2/2) du \quad (103)$$

and  $\text{SNR}_{\text{det}}(\boldsymbol{\gamma})$  is defined in equation 74. The probability of error for case 1A in equation 85 can be evaluated using (60),

$$\mu(\theta) = \left[ 1 + \frac{1}{\rho(0) \cdot \overline{\text{SNR}} \cdot (1 - \text{Re}[\rho(\theta)]/\rho(0))} \right]^{-1/2} \quad (104)$$

$$P_{e,1A}(\theta) = \left( \frac{1 - \mu(\theta)}{2} \right)^N \sum_{i=0}^{N-1} \binom{N-1+i}{i} \left( \frac{1 + \mu(\theta)}{2} \right)^i, \quad (105)$$

where  $\overline{\text{SNR}}$  is defined in equation 75.

Next, we follow similar reasoning for the LRT based on the sum of noncoherent matched filters to evaluate equations 86 and 88. We define

$$W_i \triangleq \int s_i(t)^* [\gamma_i s_i(t) + n_i(t)] dt \quad (106)$$

$$= \gamma_i \rho(0) + A_i \quad (107)$$

$$Y_i^{\text{NONCOH}}(0)^2 | H_0 = |W_i|^2 \quad (108)$$

$$X_i \triangleq \int s_i(t - \theta)^* [\gamma_i s_i(t) + n_i(t)] dt \quad (109)$$

$$= \gamma_i \rho_i(\theta) + B_i = \gamma_i \rho(\theta) + B_i \quad (110)$$

$$Y_i^{\text{NONCOH}}(\theta)^2 | H_0 = |X_i|^2, \quad (111)$$

where  $A_i, B_i$  are defined in equations 92 and 94 and are distributed as in equation 98. We have assumed  $\rho_i(\xi) = \rho(\xi)$  as in equation 46 for the rightmost equality in equation 110.

The probability of error for case 2 in equation 86 is then evaluated as

$$P_{e,2}(\theta | \boldsymbol{\gamma}) = \Pr \left\{ \sum_{i=1}^N [ |W_i|^2 - |X_i|^2 ] < 0 \right\} \quad (112)$$

where  $\boldsymbol{\gamma}$  is a deterministic parameter. For cases 2A and 3, the probabilities in equations 87 and 88 are evaluated as

$$P_{e,2A}(\theta) = P_{e,3}(\theta) = \Pr \left\{ \sum_{i=1}^N [ |W_i|^2 - |X_i|^2 ] < 0 \right\} \quad (113)$$

where  $\boldsymbol{\gamma} \sim \text{CN}(\mathbf{0}, \sigma_s^2 \mathbf{I})$ . In equations 112 and 113, the random variable  $\sum_{i=1}^N [ |W_i|^2 - |X_i|^2 ]$  is a sum of quadratic forms in which the  $N$  pairs  $(W_i, X_i)$  are complex, correlated, Gaussian random variables that are independent for  $i = 1, \dots, N$ . For

case 2 in which  $\gamma$  is deterministic, the distribution of  $(W_i, X_i)$  follows from equations 107, 110 and 98 as

$$\begin{bmatrix} W_i \\ X_i \end{bmatrix} \sim \text{CN} \left( \gamma_i \rho(0) \begin{bmatrix} 1 \\ \rho(\theta)/\rho(0) \end{bmatrix}, \rho(0) \mathcal{N}_o \begin{bmatrix} 1 & \rho(\theta)^*/\rho(0) \\ \rho(\theta)/\rho(0) & 1 \end{bmatrix} \right). \quad (114)$$

For case 3 in which  $\gamma \sim \text{CN}(\mathbf{0}, \sigma_s^2 \mathbf{I})$ , the distribution of  $(W_i, X_i)$  is

$$\begin{bmatrix} W_i \\ X_i \end{bmatrix} \sim \text{CN} \left( \mathbf{0}, \rho(0) \mathcal{N}_o [1 + \overline{\text{SNR}} \cdot \rho(0)] \begin{bmatrix} 1 & \frac{\rho(\theta)^*/\rho(0)}{1 + \overline{\text{SNR}} \cdot (\rho(\theta)/\rho(0))} \\ \rho(\theta)/\rho(0) & \frac{1 + \overline{\text{SNR}} \cdot \rho(0)}{1 + \overline{\text{SNR}} \cdot \rho(0)} \end{bmatrix} \right). \quad (115)$$

The probabilities in equations 112 and 113 can both be evaluated using the general result in (59) or (60), which is applicable with nonzero mean as in equation 114 as well as zero mean in equation 115. Both cases can be unified by a Rician fading model, in which case  $P_e$  can be obtained from (59), (60), and then equations 112 and 113 would be special cases. It would be useful to work out the Rician result, but here we restrict attention to Rayleigh fading (case 3), and equation 113 has the form (59), (60)

$$\nu(\theta) = \left[ 1 + \frac{4(1 + \overline{\text{SNR}} \cdot \rho(0))}{(\rho(0) \cdot \overline{\text{SNR}})^2 \cdot [1 - |\rho(\theta)/\rho(0)|^2]} \right]^{-1/2} \quad (116)$$

$$P_{e,3}(\theta) = \left( \frac{1 - \nu(\theta)}{2} \right)^{2N-1} \sum_{i=0}^{N-1} \binom{2N-1}{i} \left( \frac{1 + \nu(\theta)}{1 - \nu(\theta)} \right)^i. \quad (117)$$

We conclude this section by specializing the ZZB results to the FH signal model in equation 35, where  $\rho(0) = L$  from equation 45 and  $\rho(\xi) \approx L \rho_h(\xi)$  from equation 51. The ZZB for each case is numerically evaluated from equation 90 using the following  $P_e$  expressions, where the autocorrelation of the pulse shape,  $\rho_h(\xi)$ , is real-valued.

$$P_{e,1}(\theta | \gamma) = Q \left( \sqrt{L \cdot N \cdot \text{SNR}_{\text{det}}(\gamma) \cdot (1 - \rho_h(\theta))} \right) \quad (118)$$

$$\mu(\theta) = \left[ 1 + \frac{1}{L \cdot \overline{\text{SNR}} \cdot (1 - \rho_h(\theta))} \right]^{-1/2} \quad (119)$$

$$P_{e,1A}(\theta) = \left( \frac{1 - \mu(\theta)}{2} \right)^N \sum_{i=0}^{N-1} \binom{N-1+i}{i} \left( \frac{1 + \mu(\theta)}{2} \right)^i \quad (120)$$

$$\nu(\theta) = \left[ 1 + \frac{4(1 + L \cdot \overline{\text{SNR}})}{(L \cdot \overline{\text{SNR}})^2 \cdot [1 - \rho_h(\theta)^2]} \right]^{-1/2} \quad (121)$$

$$P_{e,2A}(\theta) = P_{e,3}(\theta) = \left( \frac{1 - \nu(\theta)}{2} \right)^{2N-1} \sum_{i=0}^{N-1} \binom{2N-1}{i} \left( \frac{1 + \nu(\theta)}{1 - \nu(\theta)} \right)^i. \quad (122)$$

These  $P_e$  expressions can be used to analytically approximate the SNR thresholds for TDE on parallel, fading channels. In the next section, simulation results are presented that compare the MSE performance of the MLE with the CRBs and ZZBs for various cases.

---

## 6. Examples and Simulation Results

---

This section presents numerical evaluation of the bounds (CRBs and ZZBs) for various cases, and we also compare the MSE performance of the MLE with the bounds for various scenarios. We consider the baseband FH signals as in equation 35 with symbol time is  $T_s = 10^{-3}$  s and pulse shape,  $h(t)$ , a square-root, raised-cosine with 0 excess bandwidth ( $\alpha = 0$ ). The known symbols are generated as iid QPSK sequences, and the symbol sequence on each hop is kept fixed over all simulation runs to match the model used in the analysis.

We begin by considering a single symbol per hop, so  $K = 0$  and  $L = 1$  in equation 35, which corresponds to TDE in equation 34 with signals  $s_i(t) = h(t)$  over  $N$  parallel channels. We evaluate the bounds and MLE performance as  $N$  is increased, and we show that the ZZB is a tight bound for the MSE of the MLE. Note that for this case, the signal autocorrelation in equation 51 is exact. Next, we consider the FH model in equation 35 with the total number of symbols fixed, so  $Q = LN$  is constant. The CRB depends primarily on  $Q$ , but we show that the ZZB is strongly dependent on the number of diversity channels,  $N$ , and that the CRB is not tight when  $N$  is small or when the SNR is less than a threshold value.

### 6.1 One Symbol Per Hop

Figure 2 shows the simulated MSE in comparison with the CRB and ZZB for  $K = 0$  and  $L = 1$  symbol per hop. In the legend of figure 2(c), “Coh & No Fade” corresponds to channel model case 1, “Coh & Rayleigh” corresponds to case 1A, “NonCoh & Rayleigh” corresponds to cases 2A and 3 for the ZZB, and “Rayleigh” corresponds to case 3 for the CRB. The MSE performance is shown for the MLEs in cases 1, 1A, and 3. Note in part (a) that with fading (the black and red lines) and no diversity ( $N = 1$ ), the ZZB is significantly larger than the CRB, and the CRB is not achievable at any SNR. Parts (b) and (c) show that with diversity ( $N = 3$  and 5), the ZZB converges to the CRB when the SNR exceeds a threshold, and the threshold of the ZZB is close to the threshold of the MSE, particularly for the cases of no fading (blue line) and Rayleigh fading (black line). The MSEs are computed based on 2,000 Monte Carlo runs.

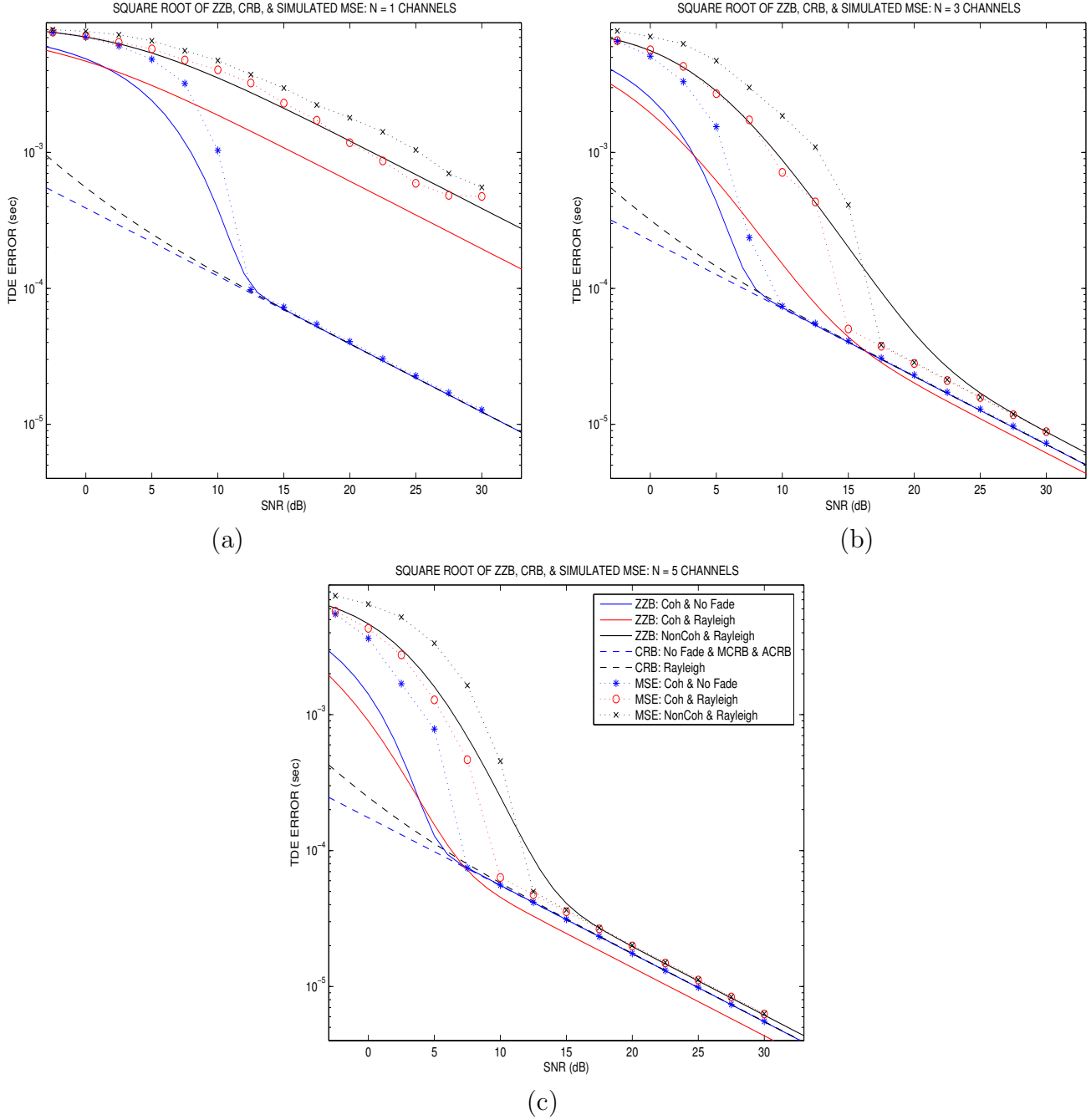


Figure 2. Comparison of CRB, ZZB, and MSE for case of  $L = 1$  symbol per hop for  $N = 1, 3,$  and  $5$  channels.

Figure 3 shows CRBs and ZZBs for the same model with  $N = 1, 2, \dots, 8$ , except that part (a) corresponds to coherent matched filters with no fading (case 1), (b) corresponds to the average of part (a) over Rayleigh channels (case 1A), and (c) corresponds to noncoherent matched filters and Rayleigh fading (case 3). Note that the SNR thresholds differ considerably in parts (a), (b), and (c). The ZZB converges to the CRB in parts (a) and (c).

In part (b), the CRB is not defined, but the MCRB and ACRB are plotted. Since there is no “true” CRB for part (b), it is not surprising that the ZZB does not converge to the  $\text{MCRB} = \text{ACRB}$ .

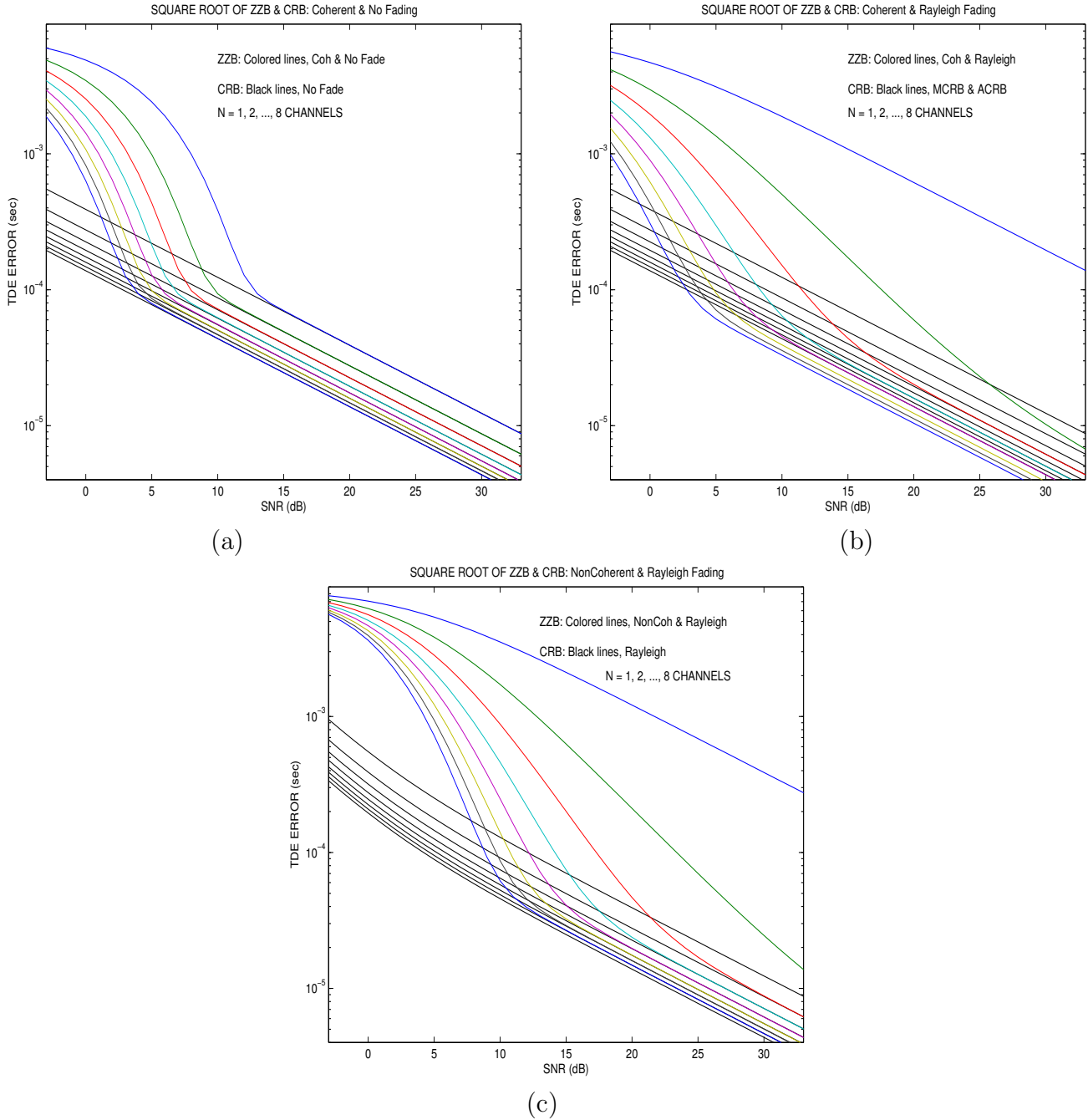


Figure 3. CRB and ZZB for case of  $L = 1$  symbol per hop for  $N = 1, 2, \dots, 8$ . (a) Known channel with fixed gain; (b) average of case (a) over Rayleigh channels, so the channel gain is known on each realization and used in a coherent matched filter; and (c) Rayleigh channels with noncoherent matched filters.

## 6.2 Multiple Symbols Per Hop

Figure 4 shows the CRB and ZZB for fixed total symbols  $Q = LN = 80$ , for  $N = 1, 2, 4, 8$  channels with  $L = 80, 40, 20, 10$  symbols per hop, respectively. Note that the CRB depends primarily on  $Q$  and varies with  $N$  only at low SNRs for the Rayleigh fading case in part (c). In part (a), with no fading and coherent matched filters, the ZZB and CRB depend only on  $Q$  and are identical as  $N$  is varied. In part (c), the ZZB changes significantly as  $N$  is varied. For  $N = 1$  with no diversity, the ZZB is much larger than the CRB. For  $N = 2, 4, 8$  in part (c), the threshold SNR decreases as the number of hops is greater. However, the difference between  $N = 4$  and  $N = 8$  is small, so the greatest diversity gain occurs with the first few additional channels.

Figures 5 and 6 contains simulation results based on 4,000 runs and 6,000 runs, respectively, to estimate the MSE using the MLE for channel model 1A in part (a) and channel model 3 in part (b). Part (b) is the case of practical interest with noncoherent matched filters and Rayleigh fading, and note that the MSE closely tracks the ZZB for  $N = 4$ , and the MSE is larger than the ZZB for  $N = 1$  and  $N = 2$ . In all cases, the ZZB is a much tighter bound than the CRB.

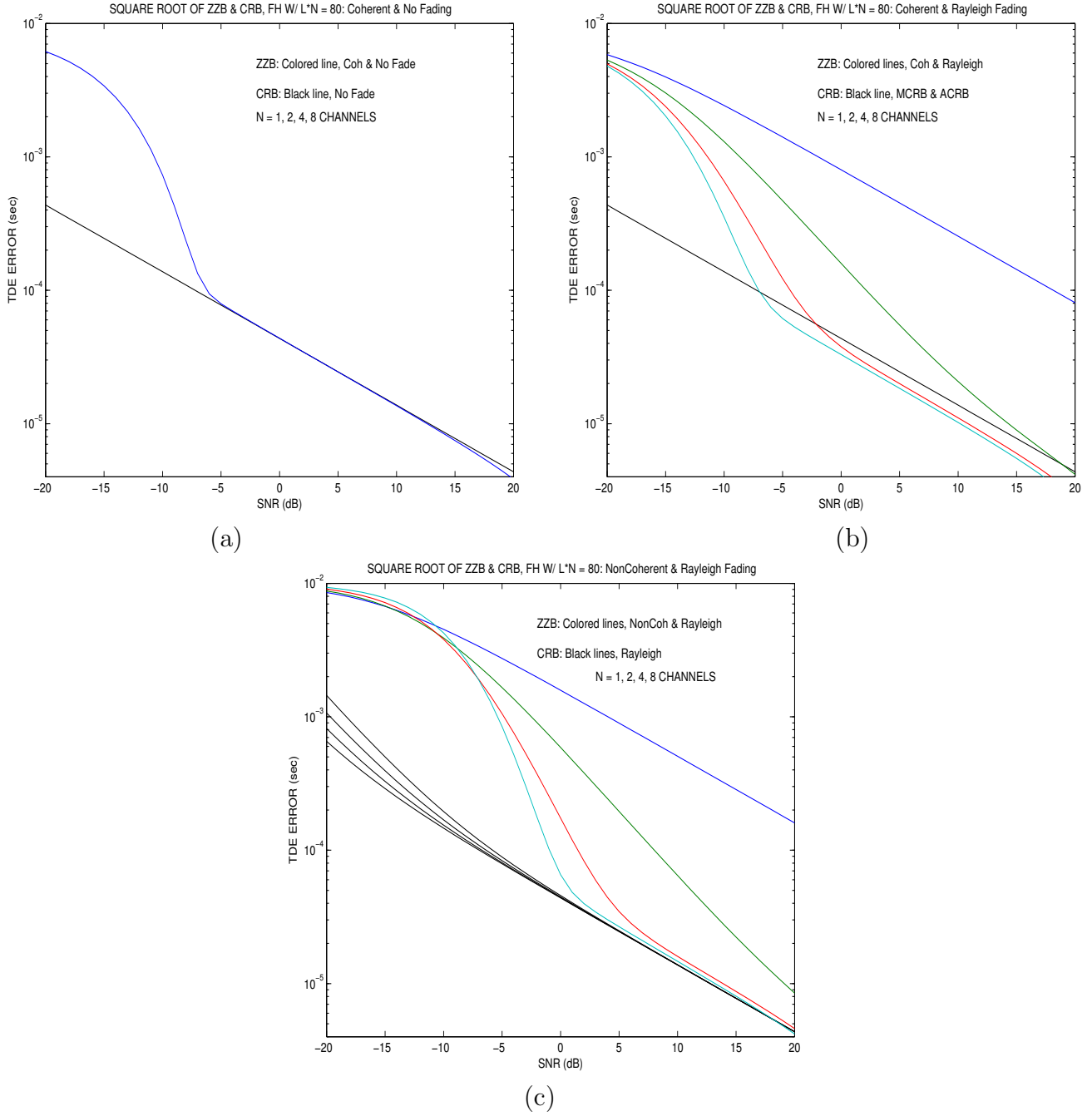


Figure 4. CRB and ZZB for fixed total number of symbols  $Q = LN = 80$ , for  $N = 1, 2, 4, 8$  so  $L = 80, 40, 20, 10$  to show the tradeoff of shorter dwells per hop and more hops. (a) Known channel with fixed gain (channel model 1); (b) average of case (a) over Rayleigh channels, so the channel gain is known on each realization and used in a coherent matched filter (channel model 1A); and (c) Rayleigh channels with noncoherent matched filters (channel model 3).

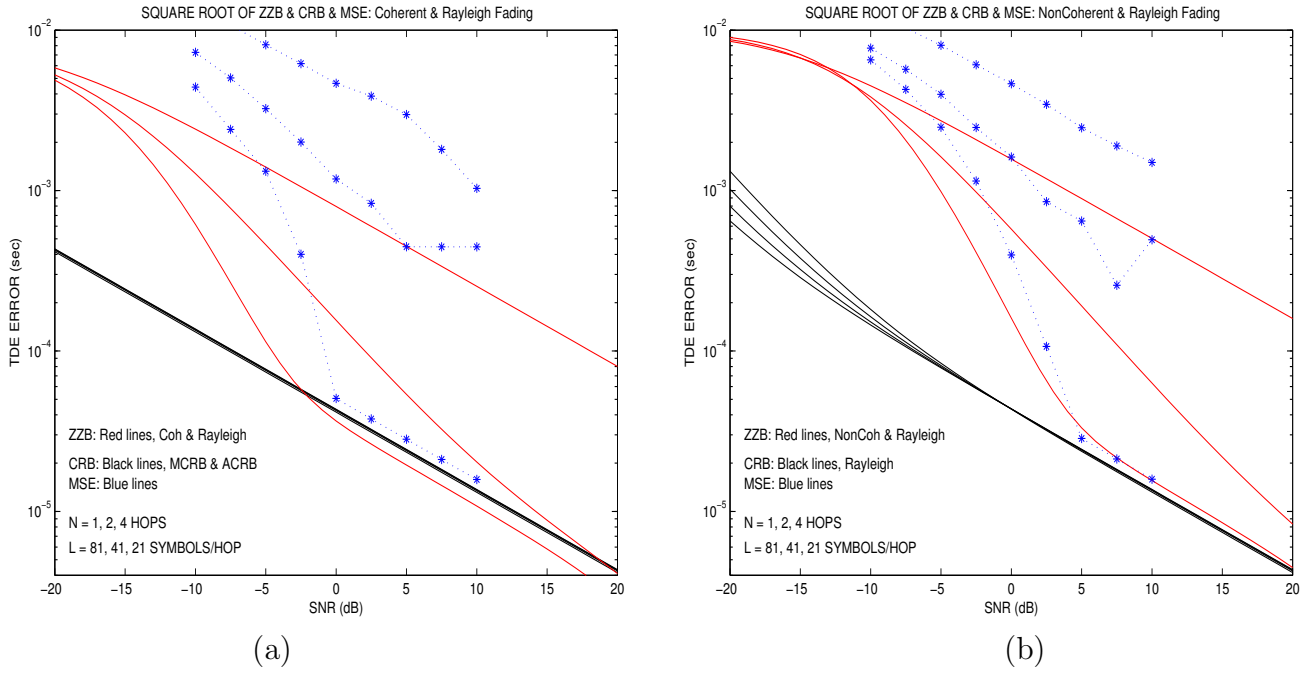


Figure 5. Comparison of CRB, ZJB, and MSE for  $Q = LN$  approximately fixed, with  $N = 1, 2, 4$  and  $L = 81, 41, 21$ . (a) Coherent matched filters, averaged over Rayleigh channel realizations (channel model 1A). (b) Noncoherent matched filters with Rayleigh fading (channel model 3). MSEs are estimated from 4,000 runs.

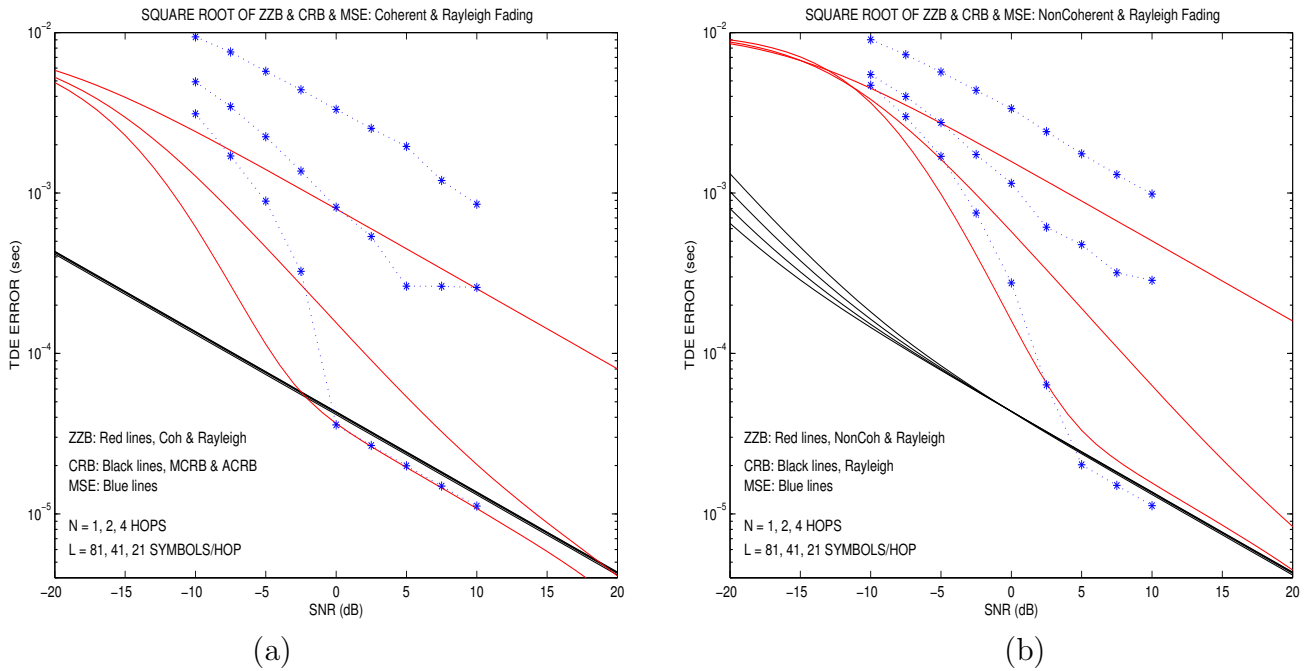


Figure 6. Comparison of CRB, ZJB, and MSE for  $Q = LN$  approximately fixed, with  $N = 1, 2, 4$  and  $L = 81, 41, 21$ . (a) Coherent matched filters, averaged over Rayleigh channel realizations. (b) Noncoherent matched filters with Rayleigh fading. MSEs are estimated from 6,000 runs.

---

## 7. Concluding Remarks

---

Several items for continued research are suggested by this work. First, it would be useful to generalize the fading model to the Rician case, and then the fixed and Rayleigh  $\gamma$  models would be special cases of the Rician model. The extension to Rician fading is straightforward based on the CRB and ZZB analysis developed in this report. Second, it would be useful to analytically characterize the threshold behavior of the ZZB with respect to SNR and the number of diversity channels,  $N$ . A simple formula would be desirable to complement the simulation results. Third, the baseband FH signal model was investigated in detail, and it will be interesting to develop corresponding results for the sum-of-tones model in equation 37.

---

## 8. References

---

1. Ash, J. N.; Moses, R. L. Acoustic Time Delay Estimation and Sensor Network Self-localization: Experimental Results. *J. Acoust. Soc. Am.* **Aug. 2005**, *118* (2), 841–850.
2. Bell, K. L.; Steinberg, Y.; Ephraim, Y.; Van Trees, H. L. Extended Ziv-Zakai Lower Bound for Vector Parameter Estimation. *IEEE Trans. Info. Theory* **March 1997**, *43* (2), 624–637.
3. Bellini, S.; Tartara, G. Bounds on Error in Signal Parameter Estimation. *IEEE Trans. Commun.* **Mar. 1974**, *COM-22*, 340–342.
4. Bellini, S.; Tartara, G. Correction to Bounds on Error in Signal Parameter Estimation. *IEEE Trans. Commun.* **Apr. 1975**, *COM-23*, 486.
5. Carey, W. M.; Moseley, W. B. Space-time Processing, Environmental-acoustic Effects. *IEEE J. of Oceanic Engineering* **July 1991**, *16* (3), 285–301.
6. Carter, G. C. *Coherence and Time Delay Estimation* (IEEE Press, 1993).
7. Cespedes, I.; Ophir, J.; Alam, S. K. The Combined Effect of Signal Decorrelation and Random Noise on the Variance of Time Delay Estimation. *IEEE Trans. on Ultrasonics, Ferroelectrics, and Frequency Control* **Jan. 1997**, *44* (1), 220–225.
8. Chazan, D.; Zakai, M.; Ziv, J. Improved Lower Bounds on Signal Parameter Estimation. *IEEE Trans. Info. Theory* **Jan. 1975**, *IT-21* (1), 90–93.
9. Chow, S.-K.; Schultheiss, P. Delay Estimation Using Narrow-band Processes. *IEEE Trans. on Acoust., Speech, and Sig. Proc.* **June 1981**, *29* (3), 478–484.
10. Ciblat, P.; Ghogho, M. Ziv-Zakai Bound for Harmonic Retrieval in Multiplicative and Additive Gaussian Noise. *Proc. 2005 IEEE Workshop on Statistical Signal Processing*, July 17–20, Bordeaux, France.
11. Friedlander, B.; Porat, B. A Parametric Technique for Time Delay Estimation. *IEEE Trans. on Aero. and Elec. Sys.* **November 1984**, *20* (6), 729–735.
12. Gini, F.; Reggiannini, R. On the Use of Cramér-Rao-Like Bounds in the Presence of Random Nuisance Parameters. *IEEE Trans. Commun.* **Dec. 2000**, *48*, 2120–2126.

13. Gini, F.; Reggiannini, R.; Mengali, U. The Modified Cramér-Rao Bound in Vector Parameter Estimation. *IEEE Trans. Comm.* **Jan. 1998**, *46* (1), 52–60.
14. Hahn, W. R. Optimum Signal Processing for Passive Sonar Range and Bearing Estimation. *J. Acoust. Soc. Am.* **July 1975**, *58* (1), 201–207.
15. Helstrom, C. W. *Elements of Signal Detection and Estimation* (Prentice-Hall, 1995).
16. Hero, A. O.; Schwartz, S. C. A New Generalized Cross Correlator. *IEEE Trans. on Acoust., Speech, and Sig. Proc.* **February 1985**, *33* (1), 38–45.
17. Huang, L.; Xu, Z.; Sadler, B. M. Ziv-Zakai Bound for Ultra-wideband Signals. *IEEE International Conference on Ultra-Wideband*, 2006 (submitted).
18. Ianniello, J. Time Delay Estimation Via Cross-correlation in the Presence of Large Estimation Errors. *IEEE Trans. on Acoust., Speech, and Sig. Proc.* **Dec. 1982**, *30* (6), 998–1003.
19. Ianniello, J.; Weinstein, E.; Weiss, A. Comparison of the Ziv-Zakai Lower Bound on Time Delay Estimation with Correlator Performance. *Proc. IEEE ICASSP '83* **Apr. 1983**, *8*, 875–878.
20. Ianniello, J. Lower Bounds on Worst Case Probability of Large Error for Two Channel Time Delay Estimation. *IEEE Trans. on Acoust., Speech, and Sig. Proc.* **Oct. 1985**, *33* (5), 1102–1110.
21. Kay, S. M. *Fundamentals of Statistical Signal Processing: Estimation Theory*; Prentice-Hall, 1993.
22. Kilfoyle, D. B.; Baggeroer, A. B. The State of the Art in Underwater Acoustic Telemetry. *IEEE J. of Oceanic Engineering* **Jan. 2000**, *25* (1), 4–27.
23. Knapp, C.; Carter, G. The Generalized Correlation Method for Estimation of Time Delay. *IEEE Trans. on Acoust., Speech, and Sig. Proc.* **Aug. 1976**, *24* (4), 320–327.
24. Kozick; R. J.; Sadler, B. M. Bounds on Time Delay and Doppler Estimation with Partially Coherent Signals. *Proc. Conf. Info. Sci. and Sys. (CISS)*, Princeton University, March 20–22, 2002.
25. Kozick; R. J.; Sadler, B. M. Source Localization with Distributed Sensor Arrays and Partial Spatial Coherence. *IEEE Trans. on Sig. Proc.* **March 2004**, *52* (3), 601–616.
26. Kozick; R. J.; Sadler, B. M. Performance of Doppler Estimation for Acoustic Sources with Atmospheric Scattering. *Proc. ICASSP*, Montreal, Canada, May 17–21, 2004.

27. Kozick; R. J.; Sadler, B. M.; Wilson, D. K. Signal Processing and Propagation for Aeroacoustic Sensor Networking. *Distributed Sensor Networks*, pp. 225–270, S.S. Iyengar and R.R. Brooks (Eds.), Chapman & Hall/CRC Press, Boca Raton, Florida, 2005.
28. Kozick; R. J.; Sadler, B. M. Sensor Localization Using Acoustic Doppler Shift with a Mobile Access Point. *Proc. IEEE Workshop on Stat. Sig. Proc. (SSP '05)*, Bordeaux, France, July 17–20, 2005.
29. Kozick; R. J.; Sadler, B. M. Frequency Hopping Waveform Diversity for Time Delay Estimation. *Proc. 2006 IEEE International Waveform Diversity & Design Conference*, Kauai, Hawaii, Jan. 22–27, 2006.
30. MacDonald, V. H.; Schultheiss, P. M. Optimum Passive Bearing Estimation in a Spatially Incoherent Noise Environment. *J. Acoust. Soc. Am.* **July 1969**, *46* (1A), 37–43.
31. McDonough, R. N.; Whalen, A. D. *Detection of Signals in Noise*; 2nd ed. (Academic Press, 1995).
32. Noels, N.; Wymeersch, H.; Steendam, H.; Moeneclaey, M. True Cramer-Rao Bound for Timing Recovery from a Bandlimited Linearly Modulated Waveform with Unknown Carrier Phase and Frequency. *IEEE Trans. Comm.* **March 2004**, *52* (3), 473–483.
33. Patwari, N.; Ash, J. N.; Kyperountas, S.; Hero, A. O.; Moses, R. L.; Correal, N. S. Locating the Nodes. *IEEE Sig. Proc. Mag.* **July 2005**, *22* (4), 54–69.
34. Prasad, S.; Narayan, M. S.; Desai, S. R. Time Delay Estimation Performance in a Scattering Medium. *IEEE Trans. on Acoust., Speech, and Sig. Proc.* **Feb. 1985**, *ASSP-33*, 50–60.
35. Raich, R.; Goldberg, J.; Messer, H. Bearing Estimation for a Distributed Source: Modeling, Inherent Accuracy Limitations and Algorithms. *IEEE Trans. on Sig. Proc.* **Feb. 2000**, *48* (2), 429–441.
36. Renaux, A.; Forster, P.; Larzabal, P. A New Derivation of the Bayesian Bounds for Parameter Estimation. *Proc. 2005 IEEE Workshop on Statistical Signal Processing*, July 17–20, Bordeaux, France.
37. Moeneclaey, M. On the True and the Modified Cramer-Rao Bounds for the Estimation of a Scalar Parameter in the Presence of Nuisance Parameters. *IEEE Trans. Commun.* **Nov. 1998**, *46*, 1536–1544.

38. Sadler, B. M.; Kozick, R. J.; Collier, S. L. Algorithms and Performance of Small Baseline Acoustic Sensor Arrays. *Proc. SPIE 2004 Defense & Security Symp.*, vol. 5417, pp. 12–23, Orlando, FL, April 12–16, 2004.
39. Scarbrough, K.; Tremblay, R.; Carter, G. Performance Predictions for Coherent and Incoherent Processing Techniques of Time Delay Estimation. *IEEE Trans. on Acoust., Speech, and Sig. Proc.* **Oct. 1983**, *31* (5), 1191–1196.
40. Schultheiss, P. M.; Messer, H.; Shor, G. Maximum Likelihood Time Delay Estimation in Non-Gaussian Noise. *IEEE Trans. on Sig. Proc.* **Oct. 1997**, *45* (10), 2571–2575.
41. Seidman, L. P. Performance Limitations and Error Calculations for Parameter Estimation. *Proc. IEEE* **May 1970**, *58*, 644–652.
42. Steendam, H.; Moeneclaey, M. Low-SNR Limit of the Cramér-Rao Bound for Estimating the Time Delay of a PAM, PSK, or QAM Waveform. *IEEE Comm. Lett.* **January 2001**, *5*, 31–33.
43. Walker, W. F.; Trahey, G. E. A Fundamental Limit on Delay Estimation Using Partially Correlated Speckle Signals. *IEEE Trans. on Ultrasonics, Ferroelectrics, and Frequency Control* **March 1995**, *42* (2), 301–308.
44. Weinstein, E.; Weiss, A. J. Lower Bounds on the Mean Square Estimation Error. *Proc. IEEE* **Sept. 1985**, *73* (9), 1433–1434.
45. Weinstein, E.; Weiss, A. J. A General Class of Lower Bounds in Parameter Estimation. *IEEE Trans. Inform. Theory* **Mar. 1988**, *34*, 338–342.
46. Weinstein, E. Relations Between Belini-Tartara, Chazan-Zakai-Ziv, and Wax-Ziv Lower Bounds. *IEEE Trans. Info. Theory* **Mar. 1988**, *34* (2), 342–343.
47. Weiss, A.; Weinstein, E. Composite Bound on the Attainable Mean Square Error in Passive Time-delay Estimation from Ambiguity Prone Signals. *IEEE Trans. Info. Theory* **Nov. 1982**, *28* (6), 977–979.
48. Weiss, A.; Weinstein, E. Fundamental Limitations in Passive Time Delay Estimation—Part I: Narrow-band Systems. *IEEE Trans. on Acoust., Speech, and Sig. Proc.* **Apr. 1983**, *31* (2), 472–486.
49. Weiss, A.; Weinstein, E. Fundamental Limitations in Passive Time-Delay Estimation—Part II: Wide-band Systems. *IEEE Trans. on Acoust., Speech, and Sig. Proc.* **Oct. 1984**, *32* (5), 1064–1078.
50. Weiss, A.; Weinstein, E. A Lower Bound on the Mean-square Error in Random Parameter Estimation. *IEEE Trans. on Info. Theory* **Sept. 1985**, *31* (5), 680–682.

51. Weiss, A. J. Composite Bounds on Arrival Time Estimation Errors. *IEEE Trans. on Aero. and Elec. Sys.* **Nov. 1986**, 22 (6), 751–756.
52. Weiss, A. J. Bounds on Time-delay Estimation for Monochromatic Signals. *IEEE Trans. on Aero. and Elec. Sys.* **Nov. 1987**, AES-23 (6), 798–808.
53. Whalen, A. D. *Detection of Signals in Noise*; (Academic Press, 1971).
54. Wilson, D. K. Performance Bounds for Acoustic Direction-of-Arrival Arrays Operating in Atmospheric Turbulence. *J. Acoust. Soc. Am.* **March 1998**, 103 (93), 1306–1319.
55. Zeira, A.; Schultheiss, P. M. Realizable Lower Bounds for Time Delay Estimation. *IEEE Trans. on Sig. Proc.* **Nov. 1993**, 41 (11), 3102–3113.
56. Zeira, A.; Schultheiss, P. M. Realizable Lower Bounds for Time Delay Estimation. 2. Threshold phenomena. *IEEE Trans. on Sig. Proc.* **May 1994**, 42 (5), 1001–1007.
57. Xu, W.; Baggeroer, A. B.; Richmond, C. D. Bayesian Bounds for Matched-field Parameter Estimation. *IEEE Trans. on Sig. Proc.* **December 2004**, 52 (12), 3293–3305.
58. Ziv, J.; Zakai, M. Some Lower Bounds on Signal Parameter Estimation. *IEEE Trans. Info. Theory* **May 1969**, IT-15 (3), 386–391.
59. Proakis, J. G. *Digital Communications*; (Third Edition), McGraw-Hill, 1995.
60. Simon, M. K.; Alouini, M.-S. *Digital Communication over Fading Channels*; (2nd Edition), Wiley, 2005.

---

## List of Symbols, Abbreviations, and Acronyms

---

ACRB	asymptotic CRB
AWGN	additive white Gaussian
BB	Barankin bound
CRB	Cramér-Rao bounds
CSD	cross-spectral density
EMCB	Extended Miller-Chang Bound
FH	frequency-hopping
FIM	Fisher Information Matrix
GCC	generalized cross-correlator
GLRT	Generalized LRT
HCRB	hybrid CRB
LL	log-likelihood
LRT	likelihood ratio test
MCRB	modified CRB
MFs	matched filters
MLE	maximum-likelihood estimator
MSE	mean-squared error
pdf	probability density function
PSD	power spectral density
RMS	root-mean-square
SNR	signal-to-noise ratio

TB	time-bandwidth
TDE	time-delay estimation
TDOA	time difference of arrival
WWBs	Weiss-Weinstein bounds
ZZB	Ziv-Zakai bound

NO OF COPIES	ORGANIZATION	NO OF COPIES	ORGANIZATION
1 ELEC	ADMNSTR DEFNS TECHL INFO CTR ATTN DTIC OCP 8725 JOHN J KINGMAN RD STE 0944 FT BELVOIR VA 22060-6218	1	US ARMY RSRCH LAB ATTN RDRL CIM G T LANDFRIED BLDG 4600 ABERDEEN PROVING GROUND MD 21005-5066
1 CD	OFC OF THE SECY OF DEFNS ATTN ODDRE (R&AT) THE PENTAGON WASHINGTON DC 20301-3080	4	US ARMY RSRCH LAB ATTN IMNE ALC HRR MAIL & RECORDS MGMT ATTN RDRL CIM L TECHL LIB ATTN RDRL CIM P TECHL PUB ATTN RDRL CIN T B SADLER ADELPHI MD 20783-1197
1	US ARMY RSRCH DEV AND ENGRG CMND ARMAMENT RSRCH DEV & ENGRG CTR ARMAMENT ENGRG & TECHNLY CTR ATTN AMSRD AAR AEF T J MATTS BLDG 305 ABERDEEN PROVING GROUND MD 21005-5001	TOTAL: 13 (1 ELEC, 1 CD, 11 HCS)	
1	PM TIMS, PROFILER (MMS-P) AN/TMQ-52 ATTN B GRIFFIES BUILDING 563 FT MONMOUTH NJ 07703		
1	US ARMY INFO SYS ENGRG CMND ATTN AMSEL IE TD A RIVERA FT HUACHUCA AZ 85613-5300		
1	COMMANDER US ARMY RDECOM ATTN AMSRD AMR W C MCCORKLE 5400 FOWLER RD REDSTONE ARSENAL AL 35898-5000		
1	US GOVERNMENT PRINT OFF DEPOSITORY RECEIVING SECTION ATTN MAIL STOP IDAD J TATE 732 NORTH CAPITOL ST NW WASHINGTON DC 20402		
1	DEPARTMENT OF ELECTRICAL ENGINEERING BUCKNELL UNIVERSITY PROFESSOR RICHARD J. KOZICK LEWISBURG, PA 17837		